X-RAY BAND DEPENDENCE OF X-RAY
TEMPERATURES IN GALAXY CLUSTERS

KENNETH W. CAVAGNOLO[1,2], MEGAN DONAHUE[1], G. MARK VOIT[1], AND MING SUN[1]
Draft version June 4, 2007

ABSTRACT

We explore the band-dependence of the inferred X-ray temperature of the intracluster medium (ICM) for NN well-observed ($N_{photons} > XX$) clusters of galaxies selected from the Chandra data archive. If the hot gas in a cluster is nearly isothermal in the projected region of interest, the X-ray temperature inferred from a broad-band (0.7-7.0 keV) spectrum should be identical to the X-ray temperature inferred from a hard-band (2-7 keV) spectrum. However, if there is excess soft X-ray photons, contributed by cooler lumps of gas or by non thermal processes, the temperature of a best-fit to a single-temperature thermal model will be cooler for a broad-band spectrum than for a hard-band spectrum. Such a diagnostic may be indicate such contamination even when the X-ray spectrum itself may not have sufficient signal-to-noise to resolve multiple temperature components. To test this possible diagnostic, we extract X-ray spectra from the annulus between $r = 70$ kpc and $r = r_{2500}$ for each cluster in our archival sample. We compare the X-ray temperatures inferred for single-temperature fits to global spectra when the energy range of the fit is 0.7-7.0 keV (total) and when the energy range is $2.0/(1+z)$ keV - 7.0 keV (hard). We find that, on average, the hard bandpass temperature is significantly higher than the full bandpass temperature. Upon further exploration, we find that the ratio is enhanced preferentially for clusters which are known merger systems and for clusters which are isothermal. Clusters with temperature decrements in their cores (known as as cool-core clusters) tend to have best-fit hard-band temperatures that are statistically consistent with their best fit full-band temperatures. We show, using simulated spectra, that this test is sensitive to cool components with emission measures $> 10\%$ ($> 5\%$) of the hot component for $Tx = 0.2 - 1.0$ keV and for $z < 0.6$. [fill in blanks.] We show that the test is relatively insensitive to second components in an individual cluster when the total counts in the spectrum is $< NNN$, but that investigation of a sample of low-count clusters may still reveal interesting trends. A comparison to the predicted distribution of temperature ratios and their relationship to putative cool lumps and/or nonthermal soft X-ray emission in cluster simulations would be very useful next step.

Subject headings: catalogs – galaxies: clusters: general – X-rays: galaxies: clusters – cosmology: observations – methods: data analysis

1. INTRODUCTION

Cluster mass functions and the evolution of the cluster mass function are useful for measuring cosmological parameters (Evrard 1989; Wang & Steinhardt 1998; Haiman et al. 2001; Hu 2003; Wang et al. 2004). Cluster evolution tests the effect of dark matter and dark energy on the evolution of dark matter halos, and therefore provide a complementary and distinct constraint on cosmological parameters to those tests which constrain them geometrically (REF) (e.g. supernovae (REF) and baryon oscillations (REF).)

However, clusters are a useful cosmological tool only if we can infer the cluster masses – the fundamental cluster property inferred from cosmological simulations (REF). from observable properties such as X-ray luminosity, X-ray temperature, lensing shear, optical luminosity, and galaxy velocity dispersion. Empirically, the relationship of mass and these observable properties is well-established (REF). However, if we could identify a "3rd parameter" – possibly reflecting the degree of relaxation in the cluster – we could improve the utility of clusters as cosmological probes.

Toward this end, we desire to understand the dynamical state of a cluster beyond identifying clusters which appear to be relaxed and those which appear to be unrelaxed. More likely, clusters have a dynamical state that is somewhere in between. The degree to which a cluster is virialized must be quantified within simulations and then observationally calibrated with an unbiased statistical sample of clusters. An ensemble of simulations of Evrard et al (XXX) were analyzed by Mathiesen & Evrard (2001) (hereafter ME01).

ME01 found clusters which had experienced a recent merger were much cooler than the cluster mass-observable scaling relations predict. They attribute this to the presence of cool, spectroscopically unresolved accreting subclusters which introduce energy into the ICM which requires a long timescale to dissipate. The consequence being an underprediction of cluster binding masses of $15 - 30\%$ (Mathiesen & Evrard 2001).

One method of quantifying the underestimate of the cluster temperature (and therefore cluster mass) employs the ratios of x-ray surface brightness moments to quantify the degree of relaxation (Buote & Tsai 1995, 1996; Jeltema et al. 2005). Although an excellent tool, power ratios suffer from being aspect dependent. ME01 found an auxiliary measure of substructure which does not depend on perspective and could be combined with power ratio to yield a more robust metric for quantifying a cluster's degree of relaxation. They found hard band (2.0_{rest}-9.0 keV) temperatures were $\sim 20\%$ hotter than broad-band (0.5-9.0 keV) temperatures. The cooler broad-band temperature was caused by unresolved accreting cool subclusters because they contribute significant amounts of line emission to the soft band ($E < 2$ keV). Work by Mazzotta et al. (2004) and Vikhlinin (2006) have confirmed this effect in simulated

[1] Department of Physics and Astronomy, Michigan State University, BPS Building, East Lansing, MI 48824
[2] cavagnolo@pa.msu.edu

Chandra and *XMM-Newton* spectra.

ME01 proposed that this effect, and consequently the fingerprint of accretion, could be detected utilizing the energy resolution and soft band sensitivity of *Chandra*. They proposed comparing single-phase temperature fits to a hard band and full band for a sufficiently large sample of clusters covering a broad dynamical range then checking for a net skew in the ratio of hard and full temperatures above unity.

In this paper we present our findings of just such a temperature ratio test using *Chandra* data. We find that on average, the hard band temperature exceeds the broad-band temperature by $\sim 13\%$ in multiple flux-limited samples of X-ray clusters from the Chandra archive. (Hereafter, we refer to hard to broad-band ratio as T_{HFR}.) This mean excess is weaker than the 20% predicted by ME01, but is significant at the 6σ level nonetheless.

This paper proceeds in the following manner. In §2 we outline sample selection criteria and *Chandra* observations selected under these criteria. Data reduction and handling of the X-ray background is discussed in §3. Spectral extraction is discussed in §4 while fitting and simulated spectra are discussed in §5. Results and discussion of our analysis are presented in §6. A final summary of our work is presented in §7. For this work we have assumed a flat ΛCDM Universe with cosmology $\Omega_M = 0.3$, $\Omega_\Lambda = 0.7$, and $H_0 = 70$ km s^{-1} Mpc^{-1}. All quoted uncertainties are at the 1.6σ level (90% confidence).

2. SAMPLE SELECTION

Our sample is selected from observations publically available in the *Chandra* X-ray Telescope's Data Archive (CDA). Our initial selection pass came from the *ROSAT* Brightest Cluster Sample (Ebeling et al. 1998), RBC Extended Sample (Ebeling et al. 2000), and *ROSAT* Brightest 55 Sample (Edge et al. 1990; Peres et al. 1998). The portion of our sample at z $\gtrsim 0.4$ can also be found in a combination of the *Einstein* Extended Medium Sensitivity Survey ((Gioia et al. 1990), North Ecliptic Pole Survey ((Henry et al. 2006), *ROSAT* Deep Cluster Survey ((Rosati et al. 1995), *ROSAT* Serendipitous Survey ((Vikhlinin et al. 1998), and Massive Cluster Survey ((Ebeling et al. 2001). Once we had a master list of possible targets, we cross-referenced this list with the CDA and gathered observations where a minimum of R_{5000} (defined below)is fully within the aimpoint CCD's field of view.

R_{Δ_c} is defined as the radius at which the average cluster density is Δ_c times the critical density of the Universe, ρ_c. For our calculations of R_{Δ_c} we adopt the relation from Arnaud et al. (2002):

$$R_{\Delta_c} = 2.71 \text{ Mpc} \cdot \beta_T \Delta_z^{-1/2} (1+z)^{3/2} \left(\frac{kT_X}{10 \text{ keV}}\right)^{1/2} \qquad (1)$$

$$\Delta_z = \frac{\Delta_c \Omega_M}{18\pi^2 \Omega_z}$$

$$\Omega_z = \frac{\Omega_M (1+z)^3}{[\Omega_M (1+z)^3] + [(1-\Omega_M - \Omega_\Lambda)(1+z)^2] + \Omega_\Lambda}$$

where R_{Δ_c} is in units of h_{70}^{-1}, Δ_c is the assumed density contrast of the cluster at R_{Δ_c}, and β_T is a numerically determined, cosmology-independent ($\lesssim \pm 20\%$) normalization for the virial relation $GM/2R = \beta_T kT$. We use $\beta_T = 1.05$ taken from Evrard et al. (1996).

The result of our CDA search is a total of 238 observations of which 158 are used from 140 clusters. The bolometric luminosities (L_{bol}) for our sample clusters plotted as a function of redshift are shown in Figure 1. Bolometric ($E \sim 0.1 - 100$) These L_{bol} values are limited to the region of the spectral extraction (from $r = 70$ kpc and $r = r_{2500}$). The location on the sky for each cluster in the sample is shown in Aitoff projection in Figure 2. [This figure is of limited relevance unless you want to show various backgrounds.

Basic properties of our sample are listed in Table 1. Fiducial temperatures and metallicities were taken from the Ph.D. thesis of Don Horner[3].

MD: THIS METHOD SHOULD BE USED (consistently) FOR ALL CLUSTERS — why use ASCA data when we're measuring temperatures ourselves???

For clusters not observed with *ASCA* and thus not listed in Horner's thesis, we used a literature search to locate values. If no published value could be located, we approximated a temperature (for the sole purpose of computing extraction regions as is discussed in §4) by recursively extracting a spectrum in the region $0.1 < r < 0.2$ R_{500} fitting a temperature and recalculating R_{500}. This process was repeated until three consecutive iterations produced R_{500} values which differed by $\leq 1\sigma$. This method of temperature determination has been employed in other studies, see Sanderson et al. (2006) and Henry et al. (2006) as examples.

3. *CHANDRA* DATA

3.1. *Reprocessing and Reduction*

All data were reduced utilizing the Chandra Interactive Analysis of Observations package (CIAO). Using `CIAO v3.3.0.1` and `CALDB v3.2.2`, standard data analysis was followed for each observation to apply the most up-to-date time-dependent gain correction and charge transfer inefficiency (CTI) correction (when appropriate)(Townsley et al. 2000). Observations taken in `VFAINT` mode had possible background events flagged using the `check_vf_pha` mode switch in `acis_process_events`.

The X-ray events were then filtered for bad grades. Only events recorded during the good time intervals (GTI) for chips were used. For observations taken prior to standard data processing version (SDP) 7.4, we flagged, inspected, and then removed the afterglow correction applied as part of the older SDP pipeline. For observations taken prior to SDP 7.4 and using `FAINT` mode, or SDP 7.6 and `VFAINT` mode, a new bad pixel file was constructed.

To detect and remove point sources we used the adaptive wavelet CIAO tool `wavdetect` (Freeman et al. 2002) on events files filtered in the energy range $0.3 - 9.0$ keV. This energy window extends below and above the energy range of interest for our spectral analysis because the photons below 0.7 keV and above 7.0 keV, while useless for diffuse emission studies, are a good diagnostic for detecting point sources (Jerius et al. 2000). After visually inspected for spurious detections or undetected sources (what the hell does this mean?) we masked these sources using 2σ ellipses as calculated from `wavdetect`. This process results in a events file (at "level 2") that has been cleaned of point sources.

Light curve analyses were then performed using Maxim Markevitch's contributed CIAO script `lc_clean.sl`[4] to check for contamination from background flares or periods of excessively high background. Periods with count rates $\geq 3\sigma$ and/or a factor ≥ 1.2 of the mean background level of the observation were removed from the GTI file. As prescribed by

---

[3] Available at http://asd.gsfc.nasa.gov/Donald.Horner/thesis.html
[4] Available at http://cxc.harvard.edu/contrib/maxim/acisbg/

Markevitch's cookbook[5], ACIS front-illuminated (FI) chips were analyzed in the $0.3 - 12.0$ keV range with time bins of 259.28 sec in length, and for the ACIS back-illuminated (BI) chips, $2.5 - 7.0$ keV energy range with time bins of 1037.12 sec.

If possible, compared light curves from a FI and BI chip in an effort to detect long duration, soft-flares which can go undetected on the FI chips but show up on the BI chips. This type of flare needs to be filtered out of the data as it introduces a spectral component which artifically increases the best-fit temperature via a high energy tail.

To determine the cluster center, we obtained the centroid of the resulting flare-clean, point-source free level-2 X-ray events file, filtered to include only photons in the $0.7 - 7.0$ keV range. Our sample includes nearly equal numbers of relaxed clusters, identified by eye, to complex clusters. (HOW WAS THIS QUANTIFIED? IF BY EYE SAY SO) For clusters which appear relaxed and azimuthally symmetric, the X-ray emission peak is nearly coincident with the emission centroid and the peak is used as the center to reduce computation time. (OF WHAT??) For clusters with noticeable substructure, the X-ray emission peak and emission centroid are not coincident and thus the centroid is adopted as the cluster center.

3.2. *X-ray Background*

Because we are attempting to measure a global temperature of clusters, specifically looking for a temperature ratio shift in energy bands which can be contaminated by the high-energy particle background or the soft local background, it is important to carefully analyze the background and subtract it from our resulting spectra.

We use blank-sky observations of the X-ray background from Markevitch et al. (2001), supplied within the CXC CALDB. First, we compare the flux from the diffuse soft X-ray background of the *ROSAT* All-Sky Survey (*RASS*) R12, R45, and R67 bands to the 0.7-7.0 keV flux in each extraction aperture for each observation. For the purpose of simplifying the subsequent analysis, we discarded observations with an R45 flux $\geq 10\%$ of the total cluster X-ray flux. MD: DEFINE , R45, R67. The appropriate blank-sky dataset for each observation was was selected from the CALDB, reprocessed exactly as the observation, and then reprojected using the aspect solutions provided with each observation. For observations on the ACIS-I array, we constructed blank-sky backgrounds for chips I0-I3 plus chips S2 and/or S3. For ACIS-S observations, we created blank-sky backgrounds only for the S3 chip plus chips I2 and/or I3. The additional off-aimpoint chips were included only if they were active during the observation and had available blank-sky data sets for the observation time period. The off-aimpoint chips were also cleaned for point sources and diffuse sources using the method outlined in §3.1.

The additional off-aimpoint chips were included in data reduction since they contain data which is farther from the cluster center and are therefore more useful in analyzing the observation background. To normalize the hard particle component we measured fluxes for identical chips in the blank-sky field and target field in the 9.5-12.0 keV range. The effective area of the ACIS arrays above 9.5 keV is zero and thus the collected photons there are exclusively from the particle background.

A histogram of the ratios of the 9.5-12.0 keV count rate from an observation's off-aimpoint chip to that of the observation specific blank-sky background are presented in Figure 3. The majority of the observations are in agreement to $\lesssim 20\%$ of the blank-sky background rate, which is small enough to not affect our analysis, however, we re-normalize all blank-sky backgrounds.

Normalization brings the observation background and blank-sky background into agreement for energies > 2 keV, but even after normalization, typically, there still exists a soft excess associated with the spatially varying soft Galactic background. Following the technique detailed in Vikhlinin et al. (2005) we construct and fit soft residuals for this component. For each observation we first compare the 0.3-2.0 keV flux of the blank-sky field and off-aimpoint field. When the off-aimpoint flux was 25% greater than the blank-sky flux, we then subtract a spectrum of the blank-sky field from a spectrum of the off-aimpoint field. The residual spectrum is fit with a solar abundance, zero redshift MeKaL model (Mewe et al. 1985, 1986; Kaastra 1992; Liedahl et al. 1995). The resulting best-fit temperatures for all of the soft background excesses identified here were between 0.2-1.0 keV, which is in agreement with results of Vikhlinin et al. (2005). The normalization of this background component was then scaled to the cluster sky area. The re-scaled component is included as a fixed background component during fitting of a cluster's spectra.

### 3.3. *Notes for Individual Clusters*

We find evidence for long duration soft flares in the observations of Abell 1758 (David & Kempner 2004), CL J2302.8+0844, and IRAS 09104+4109. These flares were handled by adding the EC CUTOFFPL/b model during spectral analysis, freezing the spectral index at $\Gamma = -0.15$, freezing the high energy exponential cut-off at 5.6 keV, and allowing the normalization to be the only free parameter. This procedure follows directly from the recommendations of Markevitch et al. (2003). IRAS 09104+4109 presented a special troubling circumstance which resulted in its removal from the sample.

4. SPECTRAL EXTRACTION

The simulated spectra calculated by ME01 were analyzed in the energy ranges $0.5 - 9.0$ keV and $2.0_{rest} - 9.0$ keV, but to make a reliable comparison with *Chandra* data we restrict our focus to a full energy band, $0.7 - 7.0$ keV, and a hard energy band, $2.0_{rest} - 7.0$ keV. We exclude data below 0.7 keV to avoid the effective area and quantum efficiency variations of the ACIS detectors, and exclude energies above 7.0 keV in which diffuse emission is dominated by the background and *Chandra*'s effective area is small. We also account for cosmic redshift by shifting our hard energy band from 2.0 keV to $2.0/(1+z)$ keV. (Henceforth, assume the 2.0 keV cut is in the rest frame unless otherwise stated.)

Mathiesen & Evrard (2001) calculated the relation between $T_{0.5-9.0}$ and $T_{2.0-9.0}$ using apertures of R_{200} and R_{500} in size. While it is trivial to calculate a temperature out to R_{200} or R_{500} from a simulation, such a measurement at these scales is extremely difficult with *Chandra* observations (see Vikhlinin et al. (2005) for a detailed explanation). However, in typical Chandra fields of view apertures with $r = R_{200}$ or even R_{500} are not fully included. Thus we chose to extract spectra from regions with radius R_{2500} when possible and R_{5000} otherwise (THIS IS RELEVANT – WHICH CLUSTERS ARE

R_{5000}???).

The cores of relaxed clusters are dominated by cool cores which affect the global temperature. Therefore we excise the central 70 kpc of each aperture. These excised apertures are denoted by "-CORE" in the text. Recent work by Maughan (2007) has shown excising 0.15 R_{500} rather than 70 kpc reduces scatter in mass-observable scaling relations but this reduction is negligible for our purposes. (WHY ✎) a check of our sensitivity to the presence of cool cores we also extract spectra for apertures with the core included. (AND THIS IN-CLUSION DEMONSTRATES THE EXPECTED EFFECT OF BLAH — this might belong in the discussion.)

Although some clusters are not circular in projection, but rather are elliptical or asymmetric, we find that extracting from a circular annulus does not significantly change the best-fit values. For another such example see Bauer et al. (2005).

After defining annular apertures, we extracted source spectra from the target cluster and background spectra from the corresponding normalized blank-sky dataset. By standard CIAO means (XXX) we created effective area functions (ARF files) and redistribution matrices (RMF files) for each cluster using a flux-weighted map (WMAP) across the entire extraction region. The WMAP was calculated over the energy range 0.3-2.0 keV to weight calibrations that vary as a function of position on the chip. Each spectrum was then binned to contain a minimum of 25 counts per channel.

5. SPECTRAL ANALYSIS

5.1. *Fitting*

Spectra were fit with XSPEC 11.3.3 (Arnaud 1996) using a single-temperature MeKaL model, in combination with the photoelectric absorption model WABS (Morrison & McCammon 1983) for Galactic absorption. Galactic absorption values, N_{HI}, are taken from Dickey & Lockman (1990). The parameters which can be fit in the WABS(MeKaL) model are N_{HI}, X-ray temperature (T_X), metallicity ($Z/Z_\odot$), and a normalization proportional to the integrated emission measure of the cluster. We fit the spectra from clusters with multiple observations simultaneously. Results from the fitting are presented in Table 4.

[WHAT ABOUT SYSTEMATIC ERROR – ANYTHING ASSUMED?]

Additional statistical error is introduced into our fitting through inclusion of the soft local background component discussed in §3.2. To account for this error we use the differences between T_X of the model using the scaled normalization and T_X of the model using $\pm 1.6\sigma$ (WHY 1.6 sigma, why not 1.0 na???) of the scaled normalization as the errors associated with this additional component. The statistical error and the error inferred from the range of normalization to the soft X-ray background component are then added in quadrature to produce a final error. In all cases this additional background error on the temperature is $< 10\%$ of the total statistical error and represents a minor inflation of the error budget.

We allowed metallicity to be free. The best-fit N_H did not differ from the Galactic value, so we fixed N_H at the Galactic value with the exception of four cases, Abell 399, (Sakelliou & Ponman 2004), Abell 520, CL 1213+0253, and MS 1008.1-1224. For the spectral fits for these clusters, we free the parameter N_H. We also find our best-fit results are robust at the 1σ level against change in aperture size (DETAILS REQUIRED FOR ME TO COMMENT OR REVISE.)

After spectral analysis we reject from our sample the datasets for the clusters 3C220.1, Abell 1682, CL 0030+2618, CL 1226.9+2153, MACS 1824.3+4309, RX J0910+5422, and RX J1053+5735 because their best-fit temperatures had no upper bound in the 90% confidence interval.

5.2. *Simulated Spectra*

To quantify the effect of a second, cooler gas component on a single-phase spectral model, we used the fakeit command within XSPEC to create an ensemble of simulated spectra for our entire sample. With these simulated spectra we are attempting to answer the question: How bright must a second temperature component be to see it in the 2.0_{rest}-7.0 over the 0.7-7.0 keV bandpass? Put another way, we are asking at what flux ratio a second gas phase skews $T_{2.0_{rest}-7.0}$ /$T_{0.7-7.0}$ to greater than unity at the 1σ level.

We began by convolving the observation-specific background, ARF, and RMF with a WABS(MeKaL$_1$+MeKaL$_2$) model for a time period equal to the observation exposure time and adding Poisson noise. We define the MeKaL$_1$ component to have the best-fit temperature and metallicity of the $R_{5000-CORE}$, 0.7-7.0 keV fit for that observation. MD: WHY R-5000??? For each realization of an observation's simulated spectrum, we vary the MeKaL$_2$ component temperature over values 0.5, 0.75, and 1.0 keV. The MeKaL$_2$ metallicity is assumed to be equal to the value of MeKaL$_1$.

We adjust the normalization of the simulated two-component spectra to achieve equivalent count rates to that in the real spectra. We explore a wide variety of K_2 by using ξ values of 0.5, 0.6, 0.7, 0.8, 0.85, 0.9, 0.95, 0.96, 0.97, 0.98, and 0.99 K_1. We simulate a control sample of single-temperature models. The control sample is essentially a simulated version of the best-fit model. This control provides us with a check of how often a hard component temperature might differ from a broad-band temperature statistically (i.e. calibration effects under control.)

For each observation, we have 53 simulated spectra, including 20 single-temperature control spectra and 33 two-component simulated spectra (three second temperatures, each with 11 different ξ). Our resulting simulated spectra ensemble contains 8374 spectra. After generating all the spectra we follow the same fitting routine for the simulated spectra as detailed in §5.1.

Plot ratio as a function of something (like best-fit Temp or z.) Line and color code the various types. Give me the final FITS file of these data if it has changed. RESULT: (1) a single temperature component rarely if ever gives significantly different temperatures if the the calibration is under control. (2) A significantly bright 2nd component must be present in order to get deviations from 1.0 as large as 1.1-1.2, as seen in the data.

[I STILL HAVE NO DISCUSSION OF THE SIMULATED SPECTRA HERE OR ELSEWHERE... MAINLY FROM NOT KNOWING WHAT TO SAY. I'LL FIND A HOME FOR THE HISTOGRAM FIGURE WHEN I WRITE THE DISCUSSION FOR THIS SECTION.]

6. RESULTS AND DISCUSSION

6.1. *Temperature Ratios*

We estimate a temperature ratio $T_{HFR} = T(2 - 7 \text{ keV})/T(0.7 - 7 \text{ keV})$ for each cluster. We find a clear departure of the mean T_{HFR} from unity for our entire sample at greater than 6σ. The weighted mean of T_{HFR} for $R_{2500-CORE}$ is 1.13 ± 0.02 and for $R_{5000-CORE}$ T_{HFR} is 1.12 ± 0.02. Presented in Figure 4 are the binned weighted-means and raw

T_{HFR} values of $R_{2500-CORE}$ and $R_{5000-CORE}$. Each bin contains 20 clusters with the exception of the highest temperature bin for $R_{5000-CORE}$ which has 14 clusters. The peculiar points with $T_{HFR} < 1$ are all statistically consistent with $T_{HFR} = 1$. Ratios less than one occur at nearly the same frequency in the control simulated dataset of single temperatures, $\sim 10-15\%$, suggesting that these ratios are consistent with statistical uncertainties in the data. (WHAT DO YOU MEAN BY THIS?? THE CONTROL SAMPLE? I MADE UP SOMETHING.)

The presence of clusters where $T_{HFR} = 1$ suggests that the calibration is not the sole reason for deviations from 1.

The uncertainty associated with each value of T_{HFR} is dominated by the larger error in $T_{2.0_{rest}-7.0}$, and on average, $\Delta T_{2.0_{rest}-7.0} \approx 2.3 \Delta T_{0.7-7.0}$. This error interval discrepency naturally results from excluding the bulk of a cluster's emission occurring below 2 keV.

We can test whether the temperature ratio depends on the best-fit broad band temperature (PLOT ratio as a function of cluster temperature) While choosing a temperature-sensitive cut-off energy for the band pass (other than 2 keV rest frame) might maintain more consistent error budget across our sample, (PLOT percentage error in the ratio as a function of cluster temperature) We do not see any systematic TREND in the ratio with cluster temperature.

(BORGANI SUGGESTS CHOOSING A CUT-OFF ENERGY BETTER MATCHED TO THE ACTUAL BEST-FIT TEMP.)

6.2. *Systematics*

Aside from instrumental and calibration effects there may be additional systematics in our analysis which do not present themselves on an individual basis but emerge as underlying trends in the sample as a whole. The three possible sources of these systematics are S/N, redshift selection, and Galactic absorption. Presented in Figure 7 are these three parameters versus T_{HFR}. The trend in T_{HFR} with redshift is expected as the 2.0/(1+z) keV hard band lower boundary nears convergence with the 0.7 keV full band lower boundary which occurs at z $\sim$ 1.85. We find no systematic trends with S/N or Galactic absorption, which might occur if the ratio offset was a consequence of poor calibration.

Shown in Figure 6 is the ratio of *ASCA* temperatures taken from Don Horner's thesis to *Chandra* temperatures derived in this work. Not all of our sample clusters have an *ASCA* temperature, but a sufficient number are available to make this comparison reliable. We note a trend of hotter *ASCA* temperatures for clusters > 10 keV. If we exclude the hottest clusters from our sample, the mean temperature ratio for the sample remains larger than one. MD:QUANTIFY

6.3. *Using T_{HFR} to Select for Relaxation*

The process of virialization may robustly result in the formation of a cool core (Ota et al. 2006). We thus ask how the presence or absence of a cool core affects T_{HFR}. Recall that we exclude the cool core itself from the cluster spectrum.

We should therefore ask about the number of cool core (CC) and non-cool core (NCC) clusters as a function of T_{HFR}. To identify a CC cluster, we extract spectra for a 50 kpc region surrounding the cluster center, then we define a temperature decrement using the ratio of temperatures for the inner 50 kpc and the $R_{5000-CORE}$ aperture, $T_{dec} = T_{50}/T_{r5000-CORE}$. If a clus-

ter's decrement was < 1 at the 2σ level then we defined it as a CC cluster, otherwise it is a NCC cluster. We then take cuts in T_{HFR} at the 1σ level and ask how many CC and NCC clusters are above these cuts.

Figure 8 shows the normalized number of CC and NCC clusters as a function of cuts in T_{HFR}. If T_{HFR} were insensitive to the dynamical state of a cluster we would expect, for normally distributed T_{HFR} values, to see the number of CC and NCC clusters monotonically decreasing. However, the number of CC clusters falls off much more rapidly than the number of NCC clusters. This effect is dramatically reduced - as expected - if the core is included. This effect indicates the contribution of soft emission is indeed playing a role in affecting T_{HFR}. This result is insensitive to our choice of significance level in both the core classification and T_{HFR} cuts.

We further define a subclass of NCC clusters as known mergers. Known mergers are NCC clusters which have identified as mergers in the cluster literature . From the figure XX we can see clusters exhibiting the highest significant values of T_{HFR} are all ongoing or recent mergers. At the 2σ level, we find increasing values of T_{HFR} favor merger systems with NCCs over relaxed, CC clusters. Mergers have left a spectroscopic imprint on the ICM which is predicted by ME01 and which we observe in our sample.

To further investigate T_{HFR} we list the identities of clusters with $T_{frac} > 1.1$ at the 1σ level. These are presented in Table 3. Of the 22 clusters, only two have CCs, Abell 907 and RX J1720.1+2638, and both have prominent cold fronts which are tell-tale signs of a subcluster merger event. The other remaining unclassified systems, MACS J1149.5+2223, RX J1525+0958, MACS J0547.0-3904, ZwCl 1215, and MACS J2311+0338 have X-ray morphologies consistent with an ongoing or post-merger scenario. Abell 1651, while relaxed in appearance, has a large, bimodal velocity dispersion indicative of a recent merger. Two clusters, Abell 1204 and MACS J1427.6-2521, show no signs of recent or ongoing merger activity, however, they reside at the bottom of the arbitrary T_{HFR} cut.

7. SUMMARY AND CONCLUSIONS

We have explored the band-dependence of the inferred X-ray temperature of the intracluster medium (ICM) for NN well-observed ($N_{counts} > XX$) clusters of galaxies selected from the Chandra data archive. All from nearly complete flux-limited samples?? We extracted spectra from the annulus between $r = 70$ kpc and $r = r_{2500}$ (and $r = r_{5000}$) for each cluster. We compare the X-ray temperatures inferred for single-temperature fits to global spectra when the energy range of the fit is 0.7-7.0 keV (total) and when the energy range is $2.0/(1+z)$ keV - 7.0 keV (hard). We find that, on average, the hard bandpass temperature is significantly higher than the full bandpass temperature. Upon further exploration, we find that the ratio is enhanced preferentially for clusters which are known merger systems and for clusters which are isothermal. Clusters with temperature decrements in their cores (known as as cool-core clusters) tend to have best-fit hard-band temperatures that are statistically consistent with their best fit full-band temperatures.

REFERENCES

Andersson, K. E., & Madejski, G. M. 2004, ApJ, 607, 190

Arnaud, K. A. 1996, in ASP Conf. Ser. 101: Astronomical Data Analysis Software and Systems V, ed. G. H. Jacoby & J. Barnes, 17–+

Arnaud, M., Aghanim, N., & Neumann, D. M. 2002, A&A, 389, 1
Arnaud, M., Hughes, J. P., Forman, W., Jones, C., Lachieze-Rey, M., Yamashita, K., & Hatsukade, I. 1992, ApJ, 390, 345
Bauer, F. E., Fabian, A. C., Sanders, J. S., Allen, S. W., & Johnstone, R. M. 2005, MNRAS, 359, 1481
Bliton, M., Rizza, E., Burns, J. O., Owen, F. N., & Ledlow, M. J. 1998, MNRAS, 301, 609
Buote, D. A., & Tsai, J. C. 1995, ApJ, 452, 522
—. 1996, ApJ, 458, 27
Burns, J. O., Roettiger, K., Pinkney, J., Perley, R. A., Owen, F. N., & Voges, W. 1995, ApJ, 446, 583
Dahle, H., Kaiser, N., Irgens, R. J., Lilje, P. B., & Maddox, S. J. 2002, ApJS, 139, 313
David, L. P., & Kempner, J. 2004, ApJ, 613, 831
Dickey, J. M., & Lockman, F. J. 1990, ARA&A, 28, 215
Ebeling, H., Edge, A. C., Allen, S. W., Crawford, C. S., Fabian, A. C., & Huchra, J. P. 2000, MNRAS, 318, 333
Ebeling, H., Edge, A. C., Bohringer, H., Allen, S. W., Crawford, C. S., Fabian, A. C., Voges, W., & Huchra, J. P. 1998, MNRAS, 301, 881
Ebeling, H., Edge, A. C., & Henry, J. P. 2001, ApJ, 553, 668
Edge, A. C., Stewart, G. C., Fabian, A. C., & Arnaud, K. A. 1990, MNRAS, 245, 559
Ettori, S., & Lombardi, M. 2003, A&A, 398, L5
Evrard, A. E. 1989, ApJ, 341, L71
Evrard, A. E., Metzler, C. A., & Navarro, J. F. 1996, ApJ, 469, 494
Feretti, L., Boehringer, H., Giovannini, G., & Neumann, D. 1997, A&A, 317, 432
Freeman, P. E., Kashyap, V., Rosner, R., & Lamb, D. Q. 2002, ApJS, 138, 185
Gioia, I. M., Maccacaro, T., Geller, M. J., Huchra, J. P., Stocke, J., & Steiner, J. E. 1982, ApJ, 255, L17
Gioia, I. M., Maccacaro, T., Schild, R. E., Wolter, A., Stocke, J. T., Morris, S. L., & Henry, J. P. 1990, ApJS, 72, 567
Girardi, M., Fadda, D., Escalera, E., Giuricin, G., Mardirossian, F., & Mezzetti, M. 1997, ApJ, 490, 56
Gómez, P. L., Hughes, J. P., & Birkinshaw, M. 2000, ApJ, 540, 726
Gutierrez, K., & Krawczynski, H. 2005, ApJ, 619, 161
Haiman, Z., Mohr, J. J., & Holder, G. P. 2001, ApJ, 553, 545
Henry, J. P., Mullis, C. R., Voges, W., Böhringer, H., Briel, U. G., Gioia, I. M., & Huchra, J. P. 2006, ApJS, 162, 304
Hu, W. 2003, Phys. Rev. D, 67, 081304
Jeltema, T. E., Canizares, C. R., Bautz, M. W., & Buote, D. A. 2005, ApJ, 624, 606
Jerius, D., Donnelly, R. H., Tibbetts, M. S., Edgar, R. J., Gaetz, T. J., Schwartz, D. A., Van Speybroeck, L. P., & Zhao, P. 2000, in Proc. SPIE Vol. 4012, p. 17-27, X-Ray Optics, Instruments, and Missions III, Joachim E. Truemper; Bernd Aschenbach; Eds., ed. J. E. Truemper & B. Aschenbach, 17–27

Kaastra, J. S. 1992
Kempner, J. C., Sarazin, C. L., & Markevitch, M. 2003, ApJ, 593, 291
Liedahl, D. A., Osterheld, A. L., & Goldstein, W. H. 1995, ApJ, 438, L115
Markevitch, M., Bautz, M. W., Biller, B., Butt, Y., Edgar, R., Gaetz, T., Garmire, G., Grant, C. E., Green, P., Juda, M., Plucinsky, P. P., Schwartz, D., Smith, R., Vikhlinin, A., Virani, S., Wargelin, B. J., & Wolk, S. 2003, ApJ, 583, 70
Markevitch, M., Govoni, F., Brunetti, G., & Jerius, D. 2005, ApJ, 627, 733
Markevitch, M., Vikhlinin, A., & Mazzotta, P. 2001, ApJ, 562, L153
Markevitch, M., Yamashita, K., Furuzawa, A., & Tawara, Y. 1994, ApJ, 436, L71
Mathiesen, B. F., & Evrard, A. E. 2001, ApJ, 546, 100
Maughan, B. J. 2007, ArXiv Astrophysics e-prints
Maughan, B. J., Jones, C., Forman, W., & Van Speybroeck, L. 2007, ArXiv Astrophysics e-prints
Mazzotta, P., Markevitch, M., Vikhlinin, A., Forman, W. R., David, L. P., & VanSpeybroeck, L. 2001, ApJ, 555, 205
Mazzotta, P., Rasia, E., Moscardini, L., & Tormen, G. 2004, MNRAS, 354, 10
Mewe, R., Gronenschild, E. H. B. M., & van den Oord, G. H. J. 1985, A&AS, 62, 197
Mewe, R., Lemen, J. R., & van den Oord, G. H. J. 1986, A&AS, 65, 511
Morrison, R., & McCammon, D. 1983, ApJ, 270, 119
Ota, N., Kitayama, T., Masai, K., & Mitsuda, K. 2006, ApJ, 640, 673
Peres, C. B., Fabian, A. C., Edge, A. C., Allen, S. W., Johnstone, R. M., & White, D. A. 1998, MNRAS, 298, 416
Rosati, P., della Ceca, R., Burg, R., Norman, C., & Giacconi, R. 1995, ApJ, 445, L11
Sakelliou, I., & Ponman, T. J. 2004, MNRAS, 351, 1439
Sanderson, A. J. R., Ponman, T. J., & O'Sullivan, E. 2006, MNRAS, 1068
Smith, G. P., Kneib, J.-P., Smail, I., Mazzotta, P., Ebeling, H., & Czoske, O. 2005, MNRAS, 359, 417
Teague, P. F., Carter, D., & Gray, P. M. 1990, ApJS, 72, 715
Townsley, L. K., Broos, P. S., Garmire, G. P., & Nousek, J. A. 2000, ApJ, 534, L139
Tucker, W., Blanco, P., Rappoport, S., David, L., Fabricant, D., Falco, E. E., Forman, W., Dressler, A., & Ramella, M. 1998, ApJ, 496, L5+
Vikhlinin, A. 2006, ApJ, 640, 710
Vikhlinin, A., Markevitch, M., Murray, S. S., Jones, C., Forman, W., & Van Speybroeck, L. 2005, ApJ, 628, 655
Vikhlinin, A., McNamara, B. R., Forman, W., Jones, C., Quintana, H., & Hornstrup, A. 1998, ApJ, 502, 558
Wang, L., & Steinhardt, P. J. 1998, ApJ, 508, 483
Wang, S., Khoury, J., Haiman, Z., & May, M. 2004, Phys. Rev. D, 70, 123008
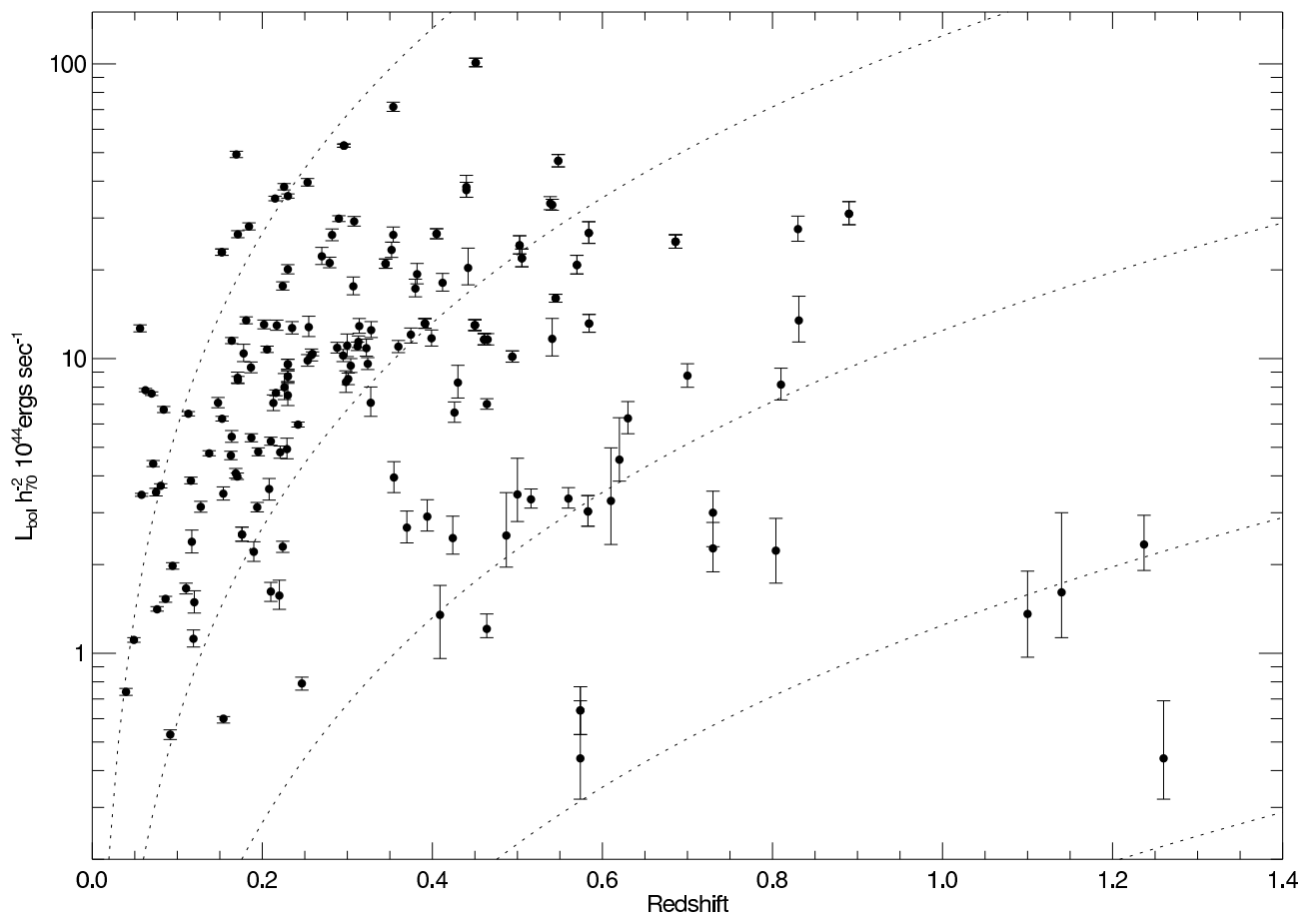
FIG. 1.— Bolometric luminosity plotted as a function of redshift for the full sample. Dotted lines represent constant fluxes of 3.0×10^{-15}, 10^{-14}, 10^{-13}, and 10^{-12} ergs sec^{-1} cm^{-2}.
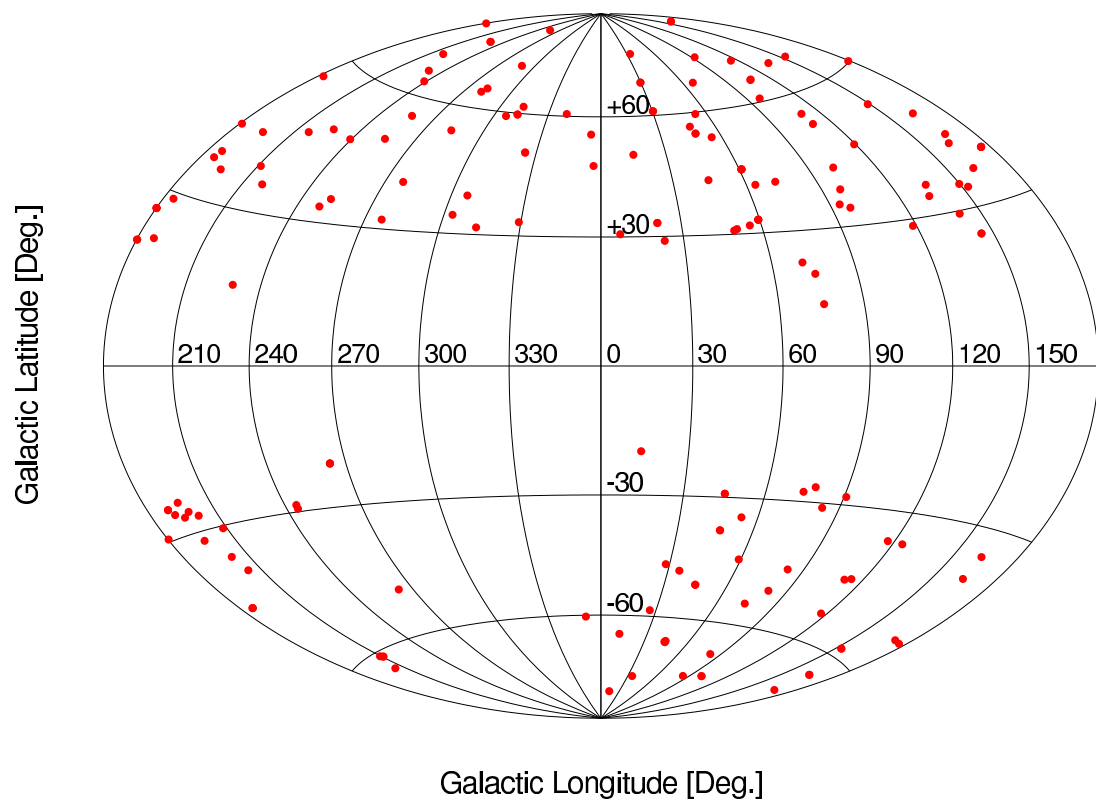
FIG. 2.— Aitoff projection of centroid for each cluster in Galactic coordinates.
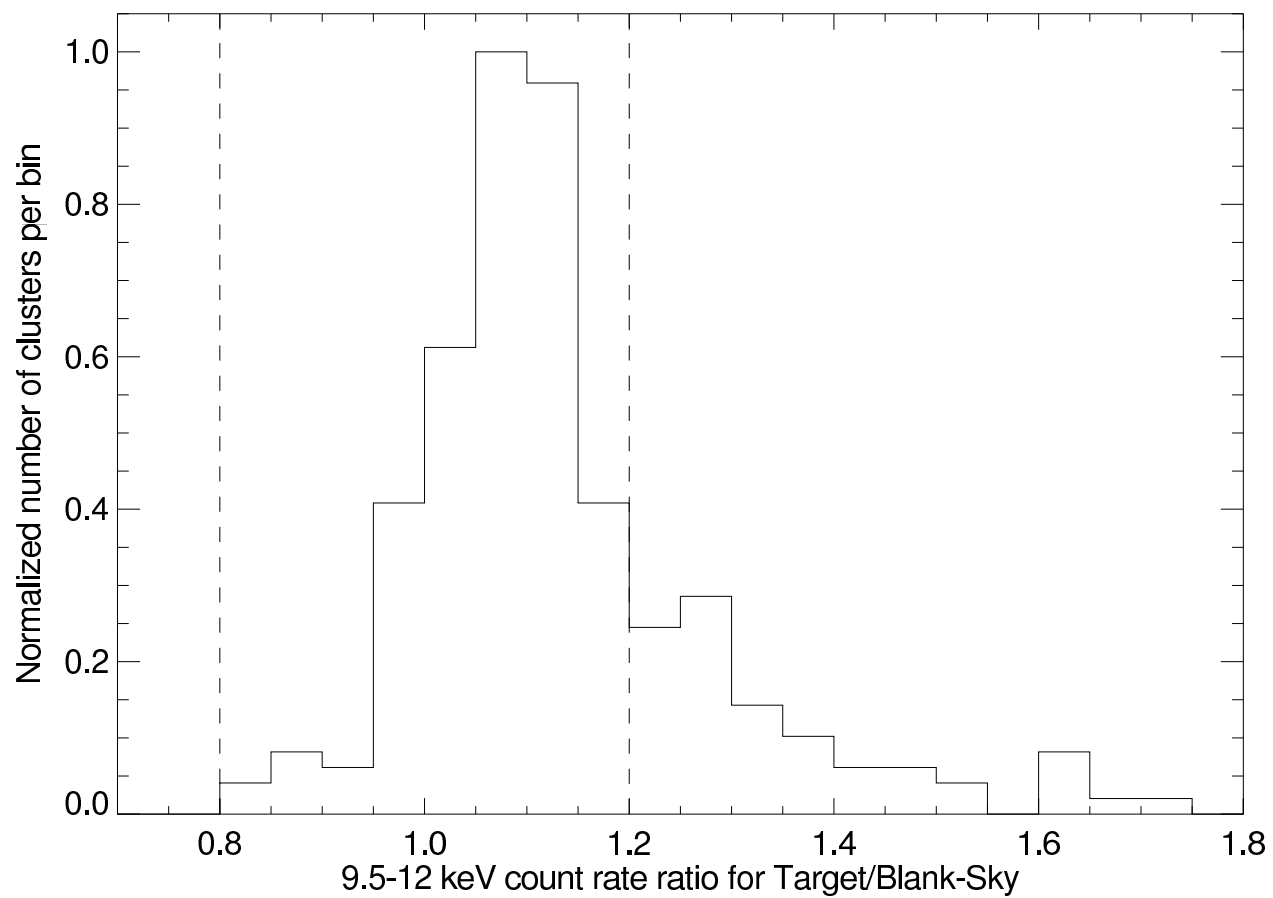
FIG. 3.— Ratio of target field and blank-sky field count rates in the 9.5-12.0 keV band for each observation. Vertical dashed lines represent ±20% of unity.
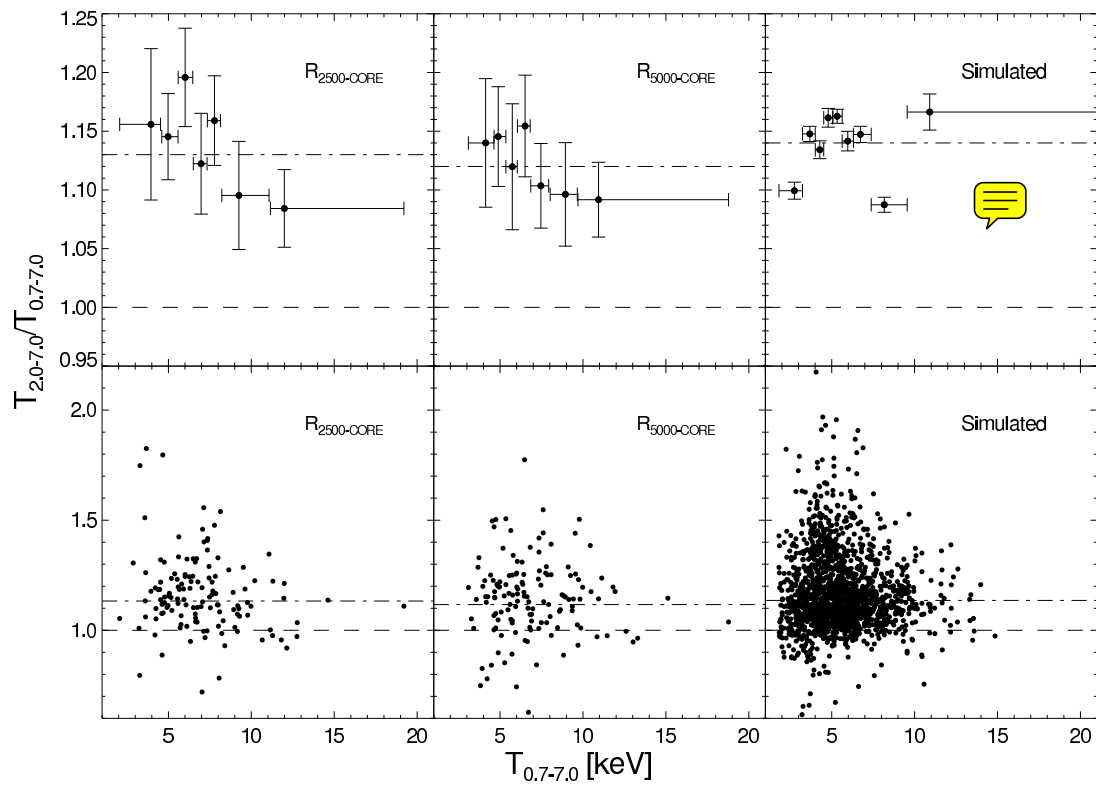
FIG. 4.— Best-fit temperatures for the hard bandpass, $T_{2.0_{rest}-7.0}$, divided by the full bandpass, $T_{0.7-7.0}$ plotted against the full bandpass temperature. For binned data, each bin contains 20 clusters, with the exception of the highest temperature bin for $R_{5000-CORE}$ which contains 14 clusters; the Simulated data bins contain 200 clusters with the last bin having 120 clusters. The line of equality is shown as a dashed line and the weighted mean for the full sample is shown as a dashed-dotted line. Error bars are omitted in the unbinned data for clarity.
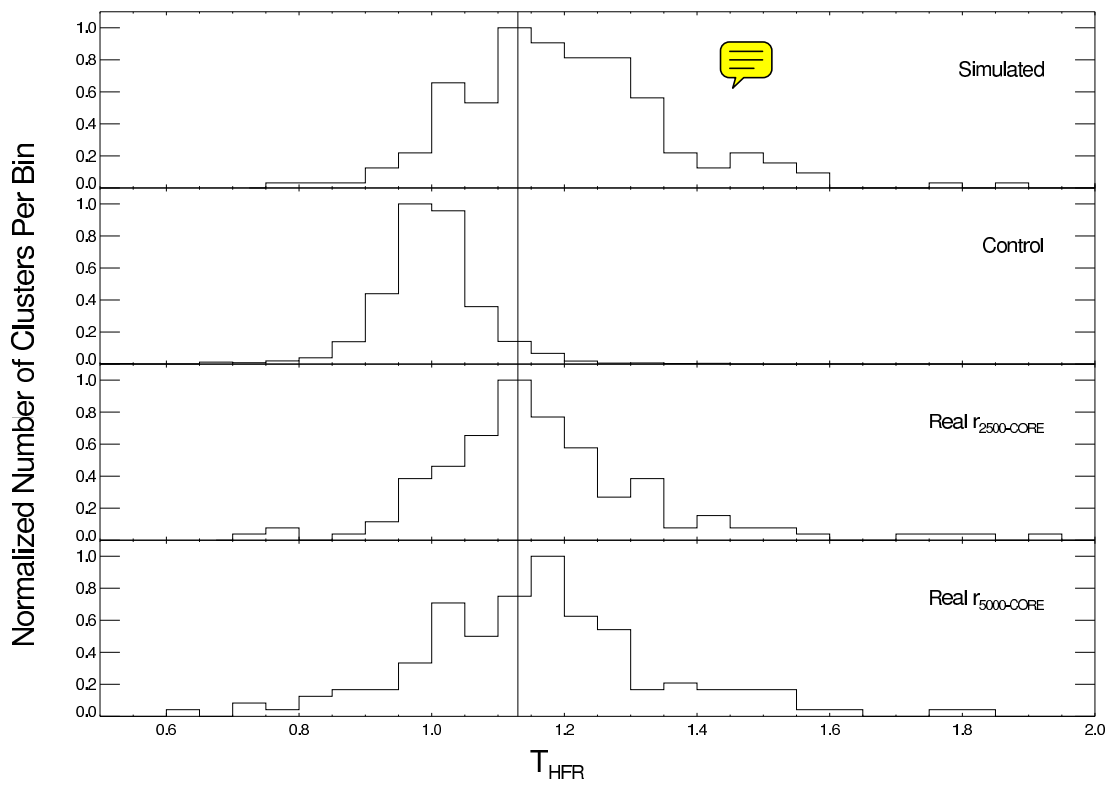
FIG. 5.— Normalized distributions for the simulated, control, $R_{2500-CORE}$, and $R_{5000-CORE}$ samples as a function of T_{HFR}. The Simulated distribution has been culled to only include spectra for $\eta = 0.9$ and $T_2 = 0.75$ keV (see §5.2 for discussion). Bins are 0.05 in width with a vertical line drawn for the weighted-mean of $T_{HFR} = 1.13$ taken from the $R_{2500-CORE}$ sample. The simulated and real distributions are nearly log-normal while the control distribution is roughly Gaussian.

Cavagnolo et al.
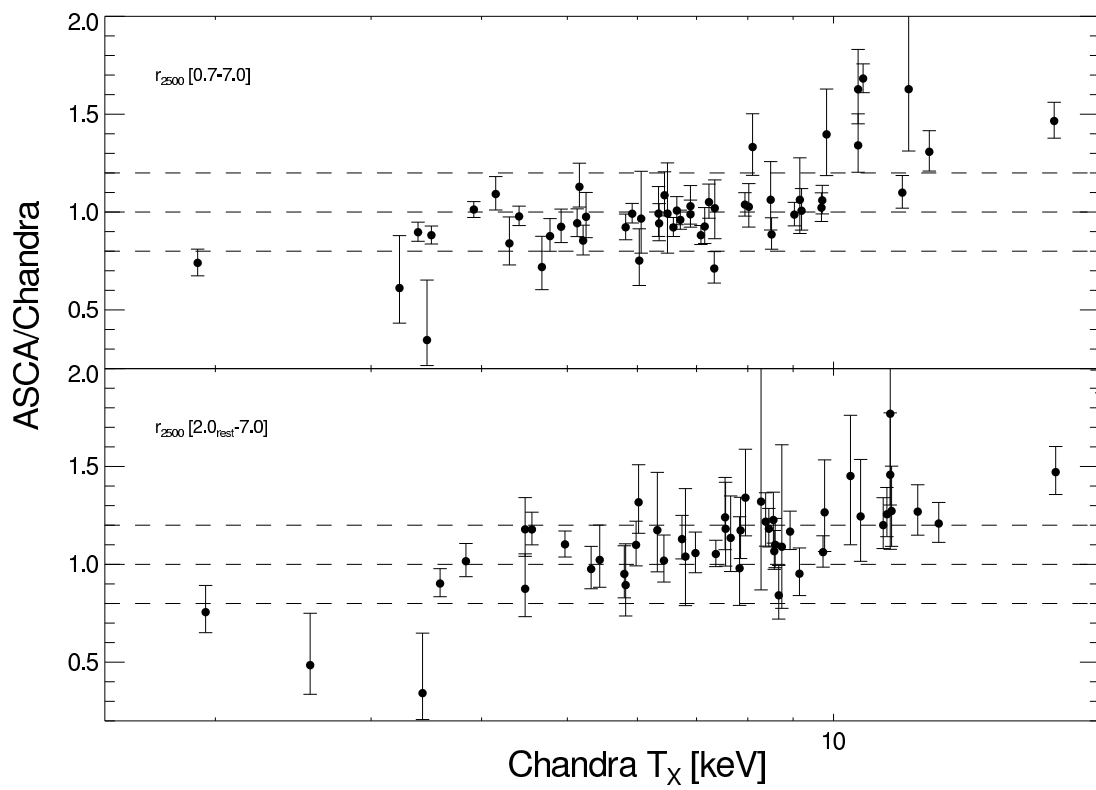
FIG. 6.— Ratio of *ASCA* temperatures taken from Don Horner's thesis to *Chandra* temperatures derived in this work. We note a trend of hotter *ASCA* temperatures for clusters > 10 keV. The spurious point below 0.5 is MS 2053.7-0449 which has a poorly constrained *ASCA* temperature. Our derived temperature of ~ 3.5 keV is in agreement with recent work of Maughan et al. (2007).
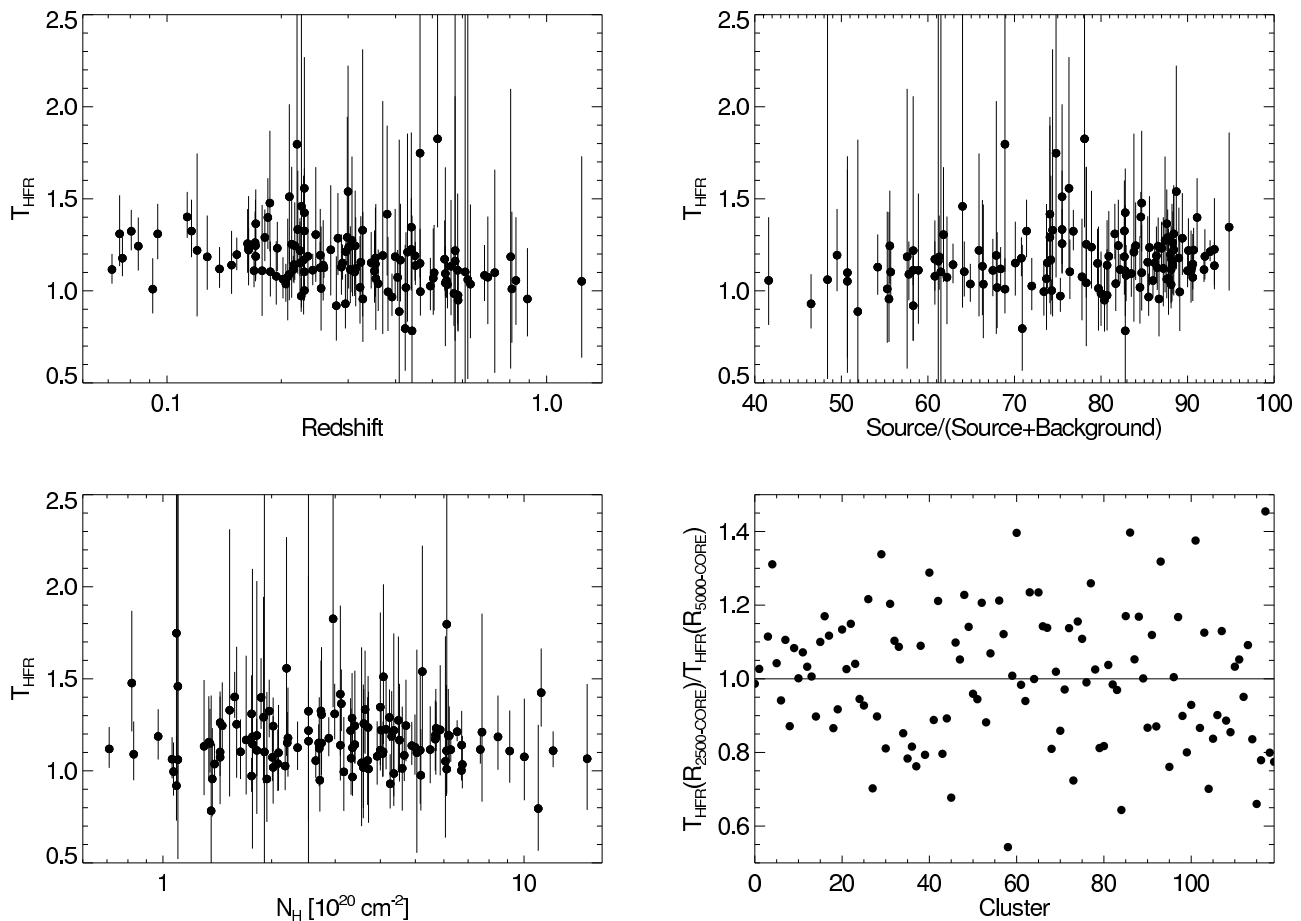
FIG. 7.— Three possible sources of systematics are plotted versus T_{HFR} plus a comparison of T_{HFR} for our two physically motivated apertures, R_{2500} and R_{5000}. Error bars have been omitted in the last plot for clarity as they all cross the line of equality. The trend in T_{HFR} with redshift is expected as the $2.0/(1+z)$ keV hard band lower boundary nears convergence with the 0.7 full band lower boundary which occurs at $z \sim 1.85$. We find no other trends in the plotted relations.
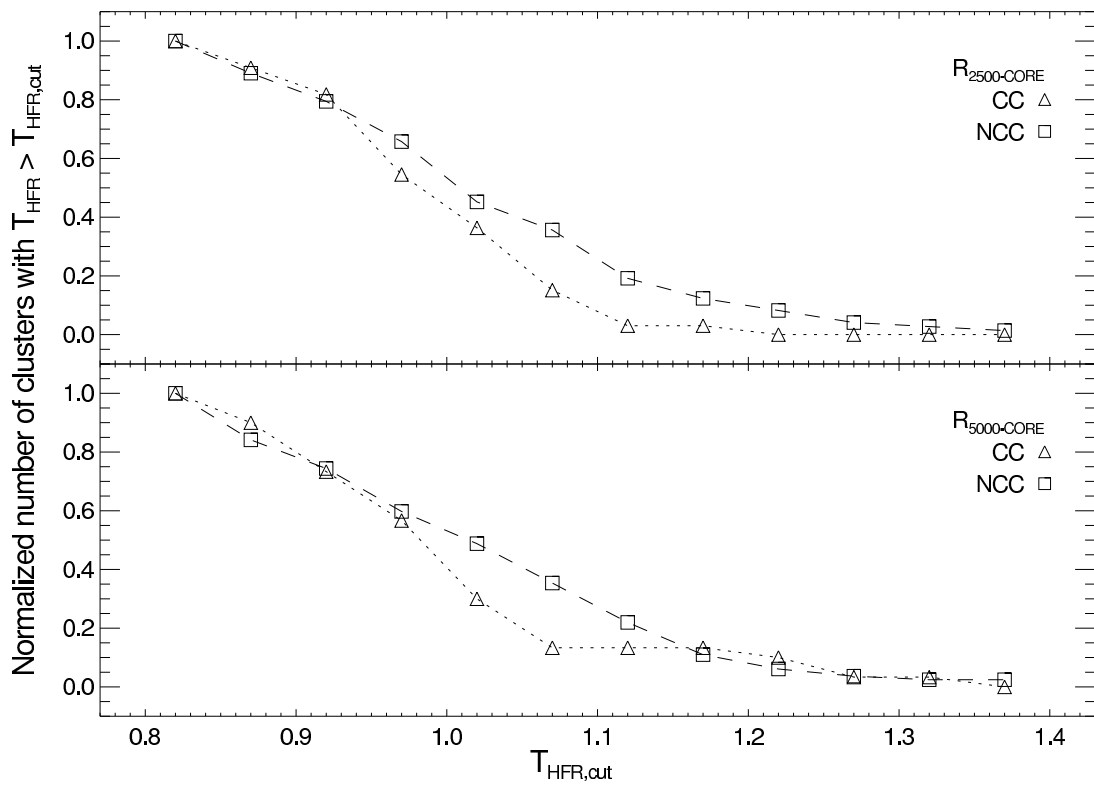
FIG. 8.— We have defined a cluster as having a cool core (CC) when the temperature for the 50 kpc around the cluster center divided by the temperature for $R_{5000–CORE}$ was less than 1 at the 2σ level. We then take cuts in T_{HFR} at the 1σ level and ask how many CC and NCC clusters are above these cuts. The number of CC clusters falls off more rapidly than NCC clusters in this classification suggesting higher values of T_{HFR} prefer less relaxed systems which do not have cool cores. This result is insensitive to our choice of significance level in both the CC classification and T_{HFR} cuts.

TABLE 1
SUMMARY OF SAMPLE

Cluster	Obs.ID	R.A. hr:min:sec	Dec. $\circ : ' : ''$	ExpT ksec	Mode	ACIS	z	$L_{bol.}$ $10^{45}\ h_{70}^{-2}$ ergs s^{-1}
(1)	(2)	(3)	(4)	(5)	(6)	(7)	(8)	(9)
1E0657 56	3184	06:58:29.510	-55:56:39.79	87.5	VF	I3	0.2960	54.10
1E0657 56	5356	06:58:29.619	-55:56:39.35	97.2	VF	I2	0.2960	54.10
1E0657 56	5361	06:58:29.436	-55:56:40.30	82.6	VF	I3	0.2960	54.10
1RXS J2129.4-0741	3199	21:29:26.274	-07:41:29.18	19.9	VF	I3	0.5700	23.30
1RXS J2129.4-0741	3595	21:29:26.016	-07:41:29.36	19.9	VF	I3	0.5700	23.30
3C 220.1	839	09:32:40.218	+79:06:29.46	18.9	F	S3	0.6100	9.67
3C 28.0	3233	00:55:50.401	+26:24:36.47	49.7	VF	I3	0.1952	5.42
3C 295	2254	14:11:20.280	+52:12:10.55	90.9	VF	I3	0.4641	10.70
3C 388	5295	18:44:02.365	+45:33:29.31	30.7	VF	I3	0.0917	0.72
4C 55.16	4940	08:34:54.923	+55:34:21.15	96.0	VF	S3	0.2420	8.01
ABELL 0068	3250	00:37:06.309	+09:09:32.28	10.0	VF	I3	0.2546	12.79
ABELL 0085	904	00:41:50.406	-09:18:10.79	38.4	F	I0	0.0558	6.44
ABELL 0133	2203	01:02:41.756	-21:52:49.79	35.5	F	S3	0.0558	1.29
ABELL 0267	1448	01:52:42.302	+01:00:44.34	7.9	F	I3	0.2300	9.10
ABELL 0267	3580	01:52:42.170	+01:00:45.63	19.9	VF	I3	0.2300	9.10
ABELL 0370	515	02:39:53.169	-01:34:36.96	88.0	F	S3	0.3747	12.45
ABELL 0383	2321	02:48:03.364	-03:31:44.69	19.5	F	S3	0.1871	7.22
ABELL 0399	3230	02:57:54.931	+13:01:58.41	48.6	VF	I0	0.0716	3.97
ABELL 0478	1669	04:13:25.345	+10:27:55.64	42.4	F	S3	0.0883	19.22
ABELL 0478	6102	04:13:25.214	+10:27:55.13	10.0	VF	I3	0.0883	19.22
ABELL 0496	3361	04:33:37.802	-13:15:40.14	10.0	VF	S3	0.0328	1.17
ABELL 0520	4215	04:54:09.711	+02:55:23.69	66.3	VF	I3	0.2020	12.20
ABELL 0521	430	04:54:07.004	-10:13:26.72	39.1	VF	S3	0.2533	9.39
ABELL 0576	3289	07:21:30.394	+55:45:41.95	38.6	VF	S3	0.0385	0.55
ABELL 0586	530	07:32:20.339	+31:37:58.59	10.0	VF	I3	0.1710	9.35
ABELL 0611	3194	08:00:56.832	+36:03:24.09	36.1	VF	S3	0.2880	12.50
ABELL 0644 †	2211	08:17:25.225	-07:30:40.03	29.7	VF	I3	0.0698	8.07
ABELL 0665	3586	08:30:59.231	+65:50:37.78	29.7	VF	I3	0.1810	13.46
ABELL 0697	4217	08:42:57.549	+36:21:57.65	19.5	VF	I3	0.2820	26.49
ABELL 0773	5006	09:17:52.566	+51:43:38.18	19.8	VF	I3	0.2170	12.88
ABELL 0781	534	09:20:25.431	+30:30:07.56	9.9	VF	I3	0.2984	7.71
ABELL 0907	3185	09:58:21.880	-11:03:52.20	48.0	VF	I3	0.1527	7.37
ABELL 0963	903	10:17:03.744	+39:02:49.17	36.3	F	S3	0.2056	12.24
ABELL 1060	2220	10:36:42.828	-27:31:42.06	31.9	VF	I3	0.0125	0.09
ABELL 1063S	4966	22:48:44.294	-44:31:48.37	26.7	VF	I3	0.3540	79.90
ABELL 1068	1652	10:40:44.520	+39:57:10.28	26.8	F	S3	0.1375	6.93
ABELL 1201 †	4216	11:12:54.489	+13:26:08.76	39.7	VF	S3	0.1688	4.51
ABELL 1204	2205	11:13:20.419	+17:35:38.45	23.6	VF	I3	0.1706	6.91
ABELL 1361 †	2200	11:43:39.827	+46:21:21.40	16.7	F	S3	0.1171	3.13
ABELL 1413	5003	11:55:17.893	+23:24:21.84	75.1	VF	I2	0.1426	11.28
ABELL 1423	538	11:57:17.026	+33:36:37.44	9.8	VF	I3	0.2130	7.40
ABELL 1650	4178	12:58:41.499	-01:45:44.32	27.3	VF	S3	0.0843	5.25
ABELL 1651	4185	12:59:22.830	-04:11:45.86	9.6	VF	I3	0.0840	7.18
ABELL 1664	1648	13:03:42.478	-24:14:44.55	9.8	VF	S3	0.1276	4.01
ABELL 1682	3244	13:06:50.764	+46:33:19.86	9.8	VF	I3	0.2260	7.23
ABELL 1689	5004	13:11:29.474	-01:20:25.17	19.9	VF	I3	0.1843	31.82
ABELL 1758	2213	13:32:42.978	+50:32:44.83	58.3	VF	S3	0.2792	19.63
ABELL 1763	3591	13:35:17.957	+40:59:55.80	19.6	VF	I3	0.1866	9.21
ABELL 1795 †	5289	13:48:52.645	+26:35:25.00	15.0	VF	I3	0.0625	9.61
ABELL 1835	495	14:01:01.951	+02:52:43.18	19.5	F	S3	0.2532	48.70
ABELL 1914	3593	14:26:01.399	+37:49:27.83	18.9	VF	I3	0.1712	28.42
ABELL 1942	3290	14:38:21.878	+03:40:12.97	57.6	VF	I2	0.2240	2.25
ABELL 1991	3193	14:54:31.620	+18:38:41.48	38.3	VF	S3	0.0565	0.77
ABELL 2029	4977	15:10:56.139	+05:44:40.96	77.9	F	S3	0.0765	18.15
ABELL 2029	6101	15:10:56.064	+05:44:40.40	9.9	VF	I3	0.0765	18.15
ABELL 2034	2204	15:10:11.003	+33:30:46.46	53.9	VF	I3	0.1130	6.29
ABELL 2069	4965	15:24:09.181	+29:53:18.05	55.4	VF	I2	0.1160	3.94
ABELL 2104	895	15:40:08.591	-03:18:07.14	49.2	F	S3	0.1554	7.40
ABELL 2111	544	15:39:41.432	+34:25:12.26	10.3	F	I3	0.2300	5.31
ABELL 2124	3238	15:44:59.131	+36:06:34.11	19.4	VF	S3	0.0658	0.52
ABELL 2125	2207	15:41:14.154	+66:15:57.20	81.5	VF	I3	0.2465	0.83
ABELL 2147	3211	16:02:13.476	+15:57:58.32	17.9	VF	I1	0.0356	0.72
ABELL 2163	1653	16:15:45.705	-06:09:00.62	71.1	VF	I1	0.1695	47.39
ABELL 2199	497	16:28:38.249	+39:33:04.28	19.5	F	S3	0.0300	1.52
ABELL 2204 †	499	16:32:46.986	+05:34:30.89	10.1	F	S3	0.1524	29.00
ABELL 2204 †	6104	16:32:46.944	+05:34:31.22	9.6	VF	I3	0.1524	29.00
ABELL 2218	1666	16:35:50.831	+66:12:42.31	48.6	VF	I0	0.1713	8.47
ABELL 2219	896	16:40:21.069	+46:42:29.07	42.3	F	S3	0.2256	39.69
ABELL 2244	4179	17:02:42.579	+34:03:37.34	57.0	VF	S3	0.0967	6.43
ABELL 2255	894	17:12:40.385	+64:03:50.63	39.4	F	I3	0.0805	6.08
ABELL 2259	3245	17:20:08.299	+27:40:11.53	10.0	VF	I3	0.1640	5.64
ABELL 2261	5007	17:22:27.254	+32:07:58.60	24.3	VF	I3	0.2240	19.71
ABELL 2294	3246	17:24:10.149	+85:53:09.77	10.0	VF	I3	0.1780	10.31

TABLE 1 — *Continued*

Cluster	Obs.ID	R.A. hr:min:sec	Dec. $^{\circ}:{}':{}''$	ExpT ksec	Mode	ACIS	z	$L_{bol.}$ $10^{45}\ h_{70}^{-2}$ ergs s^{-1}
(1)	(2)	(3)	(4)	(5)	(6)	(7)	(8)	(9)
ABELL 2319 †	3231	19:21:12.280	+43:55:57.89	14.4	VF	I1	0.0562	12.23
ABELL 2384	4202	21:52:21.178	-19:32:51.90	31.5	VF	I3	0.0945	2.14
ABELL 2390	4193	21:53:36.825	+17:41:44.38	95.1	VF	S3	0.2301	37.84
ABELL 2409	3247	22:00:52.567	+20:58:34.11	10.2	VF	I3	0.1479	7.35
ABELL 2537	4962	23:08:22.313	-02:11:29.88	36.2	VF	S3	0.2950	11.31
ABELL 2550	2225	23:11:35.806	-21:44:46.70	59.0	VF	S3	0.1543	0.83
ABELL 2554 †	1696	23:12:19.939	-21:30:09.84	19.9	VF	S3	0.1103	1.65
ABELL 2556 †	2226	23:13:01.413	-21:38:04.47	19.9	VF	S3	0.0862	2.10
ABELL 2589	3210	23:23:57.315	+16:46:38.43	13.7	VF	S3	0.0415	0.90
ABELL 2597	922	23:25:19.779	-12:07:27.63	39.4	F	S3	0.0854	3.36
ABELL 2626	3192	23:36:30.452	+21:08:47.36	24.8	VF	S3	0.0573	0.91
ABELL 2634	4816	23:38:29.397	+27:01:53.14	49.5	VF	S3	0.0314	0.06
ABELL 2667	2214	23:51:39.395	-26:05:02.75	9.6	VF	S3	0.2300	22.93
ABELL 2670	4959	23:54:13.687	-10:25:08.85	39.6	VF	I3	0.0763	1.45
ABELL 2744	2212	00:14:14.396	-30:22:40.04	24.8	VF	S3	0.3080	27.95
ABELL 3112	2516	03:17:57.681	-44:14:17.16	16.9	VF	S3	0.0720	4.68
ABELL 3158	3201	03:42:54.675	-53:37:24.36	24.8	VF	I3	0.0580	3.46
ABELL 3266	899	04:31:14.960	-61:27:32.23	29.8	VF	I1	0.0590	3.46
ABELL 3558	1646	13:27:56.854	-31:29:43.78	14.4	VF	S3	0.0480	1.96
ABELL 3562 †	4167	13:33:36.566	-31:40:27.78	19.3	VF	I2	0.0490	1.18
ABELL 3571	4203	13:47:28.434	-32:51:52.45	34.0	VF	S3	0.0391	1.86
ABELL 3667	5751	20:12:41.231	-56:50:35.70	128.9	VF	I3	0.0556	4.43
ABELL 4038	4992	23:47:44.668	-28:08:19.07	33.5	VF	I2	0.0300	1.03
AC 114	1562	22:58:48.196	-34:47:56.89	72.5	F	S3	0.3120	11.51
CL 0024+17	929	00:26:35.996	+17:09:45.37	39.8	F	S3	0.3940	3.12
CL 1221+4918	1662	12:21:26.709	+49:18:21.60	79.1	VF	I3	0.7000	8.04
CL J0030+2618	5762	00:30:33.571	+26:18:09.45	17.9	VF	I3	0.5000	3.66
CL J0152-1357	913	01:52:42.141	-13:57:59.31	36.5	F	I3	0.8310	13.58
CL J0542.8-4100	914	05:42:49.994	-40:59:58.50	50.4	F	I3	0.6300	6.73
CL J0848+4456	1708	08:48:48.235	+44:56:17.30	61.4	VF	I1	0.5740	0.73
CL J0848+4456	927	08:48:47.233	+44:56:17.13	125.1	VF	I1	0.5740	0.73
CL J1113.1-2615	915	11:13:05.167	-26:15:40.43	104.6	F	I3	0.7300	2.64
CL J1213+0253	4934	12:13:34.948	+02:53:45.45	18.9	VF	I3	0.4090	1.48
CL J1226.9+3332	3180	12:26:58.058	+33:32:46.87	31.7	VF	I3	0.8900	32.65
CL J1226.9+3332	5014	12:26:58.372	+33:32:47.67	32.7	VF	I3	0.8900	32.65
CL J1641+4001	3575	16:41:53.704	+40:01:44.40	46.5	VF	I3	0.4640	1.45
CL J2302.8+0844	918	23:02:48.156	+08:43:52.74	108.6	F	I3	0.7300	2.71
CYGNUS A	360	19:59:28.381	+40:44:01.98	34.7	F	S3	0.0561	4.03
ESO 3060170	3189	05:40:06.679	-40:50:11.97	14.1	VF	I0	0.0358	0.32
ESO 5520200	3206	04:54:52.318	-18:06:56.52	23.9	VF	I3	0.0314	0.11
EXO 0422-086 †	4183	04:25:51.271	-08:33:36.42	10.0	VF	I3	0.0397	1.02
HERCULES A †	1625	16:51:08.161	+04:59:32.44	14.8	VF	S3	0.1541	3.75
HYDRA A	4970	09:18:05.985	-12:05:43.94	98.8	VF	S3	0.0549	3.92
IRAS 09104+4109	509	09:13:45.481	+40:56:27.93	9.1	F	S3	0.4420	25.41
LYNX E	17081	08:48:58.841	+44:51:51.63	61.4	VF	I2	0.5740	0.47
LYNX E	9271	08:48:58.858	+44:51:51.46	125.1	VF	I2	1.2600	0.47
MACS J0011.7-1523	6105	00:11:42.957	-15:23:20.46	37.3	VF	I3	0.3600	13.01
MACS J0025.4-1222	3251	00:25:29.368	-12:22:38.05	19.3	VF	I3	0.5843	13.77
MACS J0025.4-1222	5010	00:25:29.332	-12:22:37.61	24.8	VF	I3	0.5843	13.77
MACS J0159.8-0849	3265	01:59:49.320	-08:50:00.41	17.9	VF	I3	0.4050	31.67
MACS J0159.8-0849	6106	01:59:49.422	-08:50:00.42	35.3	VF	I3	0.4050	31.67
MACS J0242.5-2132	3266	02:42:35.906	-21:32:26.30	11.9	VF	I3	0.3140	20.18
MACS J0257.1-2325	1654	02:57:09.130	-23:26:05.85	19.8	F	I3	0.5053	24.60
MACS J0257.1-2325	3581	02:57:09.188	-23:26:06.70	18.5	VF	I3	0.5053	24.60
MACS J0257.6-2209	3267	02:57:41.024	-22:09:11.12	20.5	VF	I3	0.3224	12.29
MACS J0329.6-0211	3257	03:29:41.616	-02:11:49.15	9.9	VF	I3	0.4500	17.70
MACS J0329.6-0211	3582	03:29:41.622	-02:11:46.82	19.9	VF	I3	0.4500	17.70
MACS J0329.6-0211	6108	03:29:41.681	-02:11:47.57	39.6	VF	I3	0.4500	17.70
MACS J0404.6+1109	3269	04:04:32.491	+11:08:02.01	21.8	VF	I3	0.3548	4.08
MACS J0417.5-1154	3270	04:17:34.686	-11:54:32.71	12.0	VF	I3	0.4400	43.38
MACS J0429.6-0253	3271	04:29:36.088	-02:53:09.02	23.2	VF	I3	0.3990	16.57
MACS J0451.9+0006	5815	04:51:54.291	+00:06:20.20	10.2	VF	I3	0.4300	9.29
MACS J0547.0-3904	3273	05:47:01.582	-39:04:28.24	21.7	VF	I3	0.2100	2.64
MACS J0717.5+3745	1655	07:17:32.443	+37:45:29.83	19.9	F	I3	0.5480	47.95
MACS J0717.5+3745	4200	07:17:31.651	+37:45:18.95	59.2	VF	I3	0.5480	47.95
MACS J0744.8+3927	3197	07:44:52.801	+39:27:25.40	20.2	VF	I3	0.6860	29.94
MACS J0744.8+3927	3585	07:44:52.779	+39:27:24.90	19.9	VF	I3	0.6860	29.94
MACS J0744.8+3927	6111	07:44:52.842	+39:27:26.28	49.5	VF	I3	0.6860	29.94
MACS J0911.2+1746	3587	09:11:11.291	+17:46:31.75	17.9	VF	I3	0.5409	12.16
MACS J0949+1708	3274	09:49:51.824	+17:07:05.62	14.3	VF	I3	0.3820	20.93
MACS J1115.8+0129	3275	11:15:52.048	+01:29:56.56	15.9	VF	I3	0.1200	2.48
MACS J1131.8-1955	3276	11:31:56.011	-19:55:55.85	13.9	VF	I3	0.3070	18.48
MACS J1149.5+2223	1656	11:49:35.466	+22:23:53.06	18.5	VF	I3	0.1761	2.76
MACS J1149.5+2223	3589	11:49:35.848	+22:23:55.04	20.0	VF	I3	0.1761	2.76

TABLE 1 — *Continued*

Cluster	Obs.ID	R.A. hr:min:sec	Dec. ° : ′ : ″	ExpT ksec	Mode	ACIS	z	$L_{bol.}$ $10^{45}\ h_{70}^{-2}$ ergs s^{-1}
(1)	(2)	(3)	(4)	(5)	(6)	(7)	(8)	(9)
MACS J1206.2-0847	3277	12:06:12.276	-08:48:02.40	23.5	VF	I3	0.4400	40.49
MACS J1226.8+2153	3590	12:26:51.207	+21:49:55.22	19.0	VF	I3	0.3700	3.21
MACS J1311.0-0310	3258	13:11:01.665	-03:10:39.50	14.9	VF	I3	0.4940	13.08
MACS J1311.0-0310	6110	13:11:01.647	-03:10:37.78	63.2	VF	I3	0.4940	13.08
MACS J1319+7003	3278	13:20:08.370	+70:04:33.81	21.6	VF	I3	0.3275	8.00
MACS J1427.6-2521	3279	14:27:39.389	-25:21:04.66	16.9	VF	I3	0.2200	2.41
MACS J1621.3+3810	3254	16:21:24.759	+38:10:07.18	9.8	VF	I3	0.4650	14.64
MACS J1621.3+3810	3594	16:21:24.933	+38:10:06.57	19.7	VF	I3	0.4610	14.64
MACS J1621.3+3810	6109	16:21:24.742	+38:10:08.92	37.5	VF	I3	0.4610	14.64
MACS J1621.3+3810	6172	16:21:24.849	+38:10:08.72	29.8	VF	I3	0.4610	14.64
MACS J1824.3+4309	3255	18:24:18.444	+43:09:43.39	14.9	VF	I3	0.4870	2.81
MACS J1931.8-2634	3282	19:31:49.656	-26:34:33.99	13.6	VF	I3	0.3520	32.00
MACS J2211.7-0349	3284	22:11:45.856	-03:49:37.24	17.7	VF	I3	0.2700	25.67
MACS J2214.9-1359	3259	22:14:57.467	-14:00:09.35	19.5	VF	I3	0.5026	26.01
MACS J2214.9-1359	5011	22:14:57.515	-14:00:10.68	18.5	VF	I3	0.5026	26.01
MACS J2228+2036	3285	22:28:33.241	+20:37:11.42	19.9	VF	I3	0.4120	19.44
MACS J2229.7-2755	3286	22:29:45.358	-27:55:38.41	16.4	VF	I3	0.3240	14.89
MACS J2245.0+2637	3287	22:45:04.547	+26:38:07.88	16.9	VF	I3	0.3040	12.19
MACS J2311+0338	3288	23:11:33.213	+03:38:06.51	13.6	VF	I3	0.2998	12.09
MKW 04	3234	12:04:27.218	+01:53:42.79	30.0	VF	S3	0.0198	0.08
MS 0016.9+1609	520	00:18:33.503	+16:26:12.99	67.4	VF	I3	0.5410	32.79
MS 0302.7+1658	525	03:05:31.614	+17:10:02.06	10.0	VF	I3	0.4240	3.22
MS 0440.5+0204 †	4196	04:43:09.952	+02:10:18.70	59.4	VF	S3	0.1900	2.95
MS 0451.6-0305	902	04:54:11.004	-03:00:52.19	44.2	F	S3	0.5386	36.16
MS 0735.6+7421	4197	07:41:44.245	+74:14:38.23	45.5	VF	S3	0.2160	8.97
MS 0839.8+2938	2224	08:42:55.969	+29:27:26.97	29.8	F	S3	0.1940	4.14
MS 0906.5+1110	924	09:09:12.753	+10:58:32.00	29.7	VF	I3	0.1630	4.88
MS 1006.0+1202	925	10:08:47.194	+11:47:55.99	29.4	VF	I3	0.2210	7.56
MS 1008.1-1224	926	10:10:32.312	-12:39:56.80	44.2	VF	I3	0.3010	12.68
MS 1054.5-0321	512	10:56:58.499	-03:37:32.76	89.1	F	S3	0.8300	27.43
MS 1455.0+2232	4192	14:57:15.088	+22:20:32.49	91.9	VF	I3	0.2590	15.00
MS 1621.5+2640	546	16:23:35.522	+26:34:25.67	30.1	F	I3	0.4260	6.95
MS 2053.7-0449	1667	20:56:21.295	-04:37:46.61	44.5	VF	I3	0.5830	2.82
MS 2053.7-0449	551	20:56:21.264	-04:37:46.80	44.3	F	I3	0.5830	2.82
MS 2137.3-2353	4974	21:40:15.178	-23:39:40.71	57.4	VF	S3	0.3130	17.51
OPHIUCHUS	3200	17:12:27.731	-23:22:06.74	50.5	F	S3	0.0280	3.90
PKS 0745-191	508	07:47:31.140	-19:17:38.98	28.0	F	S3	0.1028	24.83
PKS 0745-191	6103	07:47:31.295	-19:17:40.50	10.3	VF	I3	0.1028	24.83
RBS 0797	2202	09:47:12.971	+76:23:13.90	11.7	VF	I3	0.3540	37.93
RDCS 1252-29	4198	12:52:54.221	-29:27:21.01	163.4	VF	I3	1.2370	2.80
RX J0439+0520	527	04:39:02.218	+05:20:43.11	9.6	VF	I3	0.2080	5.45
RX J0439.0+0715	1449	04:39:00.710	+07:16:08.15	6.3	F	I3	0.2300	10.98
RX J0439.0+0715	3583	04:39:00.710	+07:16:07.82	19.2	VF	I3	0.2300	10.98
RX J0647.7+7015	3196	06:47:50.029	+70:14:50.15	19.3	VF	I3	0.5840	27.91
RX J0647.7+7015	3584	06:47:49.919	+70:14:54.91	20.0	VF	I3	0.5840	27.91
RX J0819.6+6336 †	2199	08:19:26.007	+63:37:26.53	14.9	F	S3	0.1190	1.27
RX J0820.9+0752	1647	08:21:02.180	+07:51:48.42	9.4	F	S3	0.1100	1.01
RX J0910+5422	2452	09:10:44.478	+54:22:04.26	65.3	VF	I3	1.1000	1.48
RX J1053+5735	4936	10:53:39.844	+57:35:18.42	92.2	F	S3	1.1400	2.44
RX J1347.5-1145	3592	13:47:30.593	-11:45:10.05	57.7	VF	I3	0.4510	125.14
RX J1347.5-1145	507	13:47:30.632	-11:45:09.78	10.0	F	S3	0.4510	125.14
RX J1350+6007	2229	13:50:48.038	+60:07:08.39	58.3	VF	I3	0.8040	2.38
RX J1423.8+2404	1657	14:23:47.759	+24:04:40.95	18.5	VF	I3	0.5450	23.77
RX J1423.8+2404	4195	14:23:47.942	+24:04:43.09	115.6	VF	S3	0.5450	23.77
RX J1504.1-0248	5793	15:04:07.415	-02:48:15.70	39.2	VF	I3	0.2150	51.25
RX J1525+0958	1664	15:24:39.729	+09:57:44.42	50.9	VF	I3	0.5160	3.41
RX J1532.9+3021	1649	15:32:53.781	+30:20:58.72	9.4	VF	S3	0.3450	28.34
RX J1532.9+3021	1665	15:32:53.817	+30:20:58.34	10.0	VF	I3	0.3450	28.34
RX J1716.9+6708	548	17:16:49.015	+67:08:25.80	51.7	F	I3	0.8100	9.00
RX J1720.1+2638	4361	17:20:09.941	+26:37:29.11	25.7	VF	I3	0.1640	14.50
RX J1720.2+3536	3280	17:20:16.792	+35:36:26.08	20.8	VF	I3	0.3913	16.44
RX J1720.2+3536	6107	17:20:16.908	+35:36:26.43	33.9	VF	I3	0.3913	16.44
RX J1720.2+3536	7225	17:20:16.947	+35:36:23.78	2.0	VF	I3	0.3913	16.44
RX J2129.6+0005	552	21:29:39.944	+00:05:18.83	10.0	VF	I3	0.2350	14.82
SERSIC 159-03	1668	23:13:58.764	-42:43:34.70	9.9	VF	S3	0.0580	1.97
V 1121.0+2327	1660	11:20:57.195	+23:26:27.60	71.3	VF	I3	0.5600	3.13
ZWCL 1215	4184	12:17:40.787	+03:39:39.42	12.1	VF	I3	0.0750	3.71
ZWCL 1358+6245	516	13:59:50.526	+62:31:04.57	54.1	F	S3	0.3280	13.45
ZWCL 1953	1659	08:50:06.677	+36:04:16.16	24.9	F	I3	0.3800	18.30
ZWCL 3146	909	10:23:39.735	+04:11:08.05	46.0	F	I3	0.2900	43.20
ZWCL 5247	539	12:34:21.928	+09:47:02.83	9.3	VF	I3	0.2290	4.57
ZWCL 7160	543	14:57:15.158	+22:20:33.85	9.9	F	I3	0.2578	15.09
ZWICKY 2701	3195	09:52:49.183	+51:53:05.27	26.9	VF	S3	0.2100	6.61
ZwCL 1332.8+5043	5772	13:34:20.698	+50:31:04.64	19.5	VF	I3	0.6200	4.82

TABLE 1 — *Continued*

Cluster	Obs.ID	R.A. hr:min:sec	Dec. ° : ′ : ″	ExpT ksec	Mode	ACIS	z	$L_{bol.}$ $10^{45}\ h_{70}^{-2}$ ergs s^{-1}
(1)	(2)	(3)	(4)	(5)	(6)	(7)	(8)	(9)

NOTE. — (1) Cluster name, (2) CDA observation identification number, (3) centroid R.A., (4) centroid Dec., (5) nominal exposure time, (6) observing mode, (7) CCD location of centroid, (8) redshift, (9) NRAO absorbing Galactic neutral hydrogen column density, (10) fiducial temperature, (11) fiducial abundance, (12) bolometric luminosity. † indicates clusters analyzed within r$_{5000}$ only.

TABLE 2
WEIGHTED AVERAGES FOR VARIOUS APERTURES

Aperture	[0.7-7.0] keV	[2.0$_{rest}$-7.0] keV	T_{HFR}	[0.7-7.0] keV	[2.0$_{rest}$-7.0] keV	T_{HFR}
	. . . . Without Core			. . . . With Core		
R$_{2500}$	5.50±0.04	6.95±0.09	1.14±0.02	4.71±0.03	5.79±0.06	1.11±0.01
R$_{5000}$	5.29±0.03	6.83±0.09	1.12±0.02	4.72±0.02	6.05±0.07	1.13±0.01
Simulated	3.12±0.004	4.60±0.009	1.13±0.002	. . . .	. . . .	. . . .

TABLE 3
CLUSTERS WITH T$_{frac}$ > 1.1 AT THE 1σ LEVEL.

Name	T_{HFR}	Merger	Core	X-ray Morphology	Ref.
MACS J1149.5+2223	$1.92^{+0.78}_{-0.47}$	L	NCC	"Persian Pickle"	none
MS 1008.1-1224	$1.62^{+0.39}_{-0.28}$	Y	NCC	Two subclusters w/ gas tail	[1]
RX J1525+0958	$1.83^{+0.79}_{-0.48}$	L	NCC	Arrowhead	none
Abell 2034	$1.40^{+0.14}_{-0.11}$	Y	NCC	Relaxed w/ cold front	[2]
Abell 520	$1.40^{+0.13}_{-0.12}$	Y	NCC	Boot shaped cool wake	[3]
Abell 1689	$1.40^{+0.21}_{-0.17}$	Y	NCC	Relaxed	[4],[5]
Abell 2255	$1.32^{+0.12}_{-0.10}$	Y	NCC	Relaxed	[6],[7]
Abell 2218	$1.36^{+0.19}_{-0.15}$	Y	NCC	Relaxed	[8]
Abell 1763	$1.48^{+0.39}_{-0.26}$	Y	NCC	Elongated	[9],[10]
Abell 2069	$1.32^{+0.17}_{-0.14}$	Y	NCC	Elongated	[11]
Abell 2384	$1.31^{+0.16}_{-0.14}$	Y	NCC	Elongated w/ gas tail	none
1E0657-56	$1.21^{+0.06}_{-0.05}$	Y	NCC	"Bullet Cluster"	[18]
Abell 665	$1.29^{+0.15}_{-0.13}$	Y	NCC	Prominent cold front	[12]
MACS J0547.0-3904	$1.51^{+0.50}_{-0.36}$	L	NCC	Asymmetric	none
Abell 2163	$1.25^{+0.13}_{-0.11}$	Y	NCC	Hottest cluster known	[13],[14]
ZwCl 1215	$1.31^{+0.21}_{-0.17}$	L	NCC	Elongated	none
Abell 1204	$1.26^{+0.17}_{-0.14}$	N	NCC	Relaxed w/o cold front	none
MACS J2311+0338	$1.54^{+0.68}_{-0.42}$	L	NCC	Elongated	none
RX J1720.1+2638	$1.22^{+0.12}_{-0.11}$	Y	CC	Relaxed w/ cold front	[15]
Abell 907	$1.20^{+0.09}_{-0.08}$	L	CC	Relaxed w/ cold front	none
Abell 1651	$1.24^{+0.16}_{-0.13}$	L	NCC	Relaxed w/ large vel. dispersion	[16]
3C28.0 (Abell 115) .	$1.23^{+0.14}_{-0.12}$	Y	NCC	Two subclusters w/ gas tail	[17]
MACS J1427.6-2521	$1.80^{+1.13}_{-0.69}$	N	NCC	Relaxed w/o cold front	none

NOTE. — Clusters ordered by lower limit of T_{HFR}. [1] Ettori & Lombardi (2003), [2] Kempner et al. (2003), [3] Markevitch et al. (2005), [4] Teague et al. (1990), [5] Andersson & Madejski (2004), [6] Burns et al. (1995), [7] Feretti et al. (1997), [8] Girardi et al. (1997), [9] Dahle et al. (2002), [10] Smith et al. (2005), [11] Gioia et al. (1982), [12] Gómez et al. (2000), [13] Arnaud et al. (1992), [14] Markevitch et al. (1994), [15] Mazzotta et al. (2001), [16] Bliton et al. (1998), [17] Gutierrez & Krawczynski (2005), [18] Tucker et al. (1998).

TABLE 4
SUMMARY OF EXCISED R$_{2500}$ SPECTRAL FITS

Cluster	N_H 10^{20} cm^{-2}	T_{77} keV	T_{27} keV	T_{HFR}	Z_{77} $Z_{\odot}$	$\chi^2_{red,77}$	$\chi^2_{red,27}$	% Source
(1)	(2)	(3)	(4)	(5)	(6)	(7)	(8)	(9)
1E0657 56 †	6.53	$11.99^{+0.27}_{-0.26}$	$14.54^{+0.67}_{-0.53}$	$1.21^{+0.06}_{-0.05}$	$0.29^{+0.03}_{-0.02}$	1.24	1.11	92.6
1RXS J2129.4-0741 †	4.36	$8.22^{+1.18}_{-0.95}$	$8.10^{+1.47}_{-1.10}$	$0.99^{+0.23}_{-0.18}$	$0.43^{+0.18}_{-0.17}$	1.07	1.05	80.0
3C 220.1	1.91	$6.51^{+6.73}_{-2.72}$	$7.18^{+17.56}_{-3.77}$	$1.10^{+2.93}_{-0.74}$	$0.00^{+0.60}_{-0.00}$	1.15	1.39	61.5
3C 28.0	5.71	$5.53^{+0.29}_{-0.27}$	$6.81^{+0.71}_{-0.60}$	$1.23^{+0.12}_{-0.12}$	$0.30^{+0.08}_{-0.07}$	0.98	0.88	87.0
3C 295	1.35	$5.16^{+0.42}_{-0.38}$	$5.93^{+0.84}_{-0.69}$	$1.15^{+0.19}_{-0.16}$	$0.38^{+0.12}_{-0.11}$	0.91	0.93	79.6
3C 388	6.11	$3.23^{+0.23}_{-0.21}$	$3.26^{+0.49}_{-0.37}$	$1.01^{+0.19}_{-0.13}$	$0.51^{+0.16}_{-0.14}$	0.95	0.95	68.9
4C 55.16	4.00	$4.98^{+0.17}_{-0.17}$	$5.54^{+0.40}_{-0.36}$	$1.11^{+0.09}_{-0.08}$	$0.49^{+0.07}_{-0.07}$	0.89	0.80	58.3
ABELL 0068	4.60	$9.01^{+1.53}_{-1.14}$	$9.13^{+2.60}_{-1.71}$	$1.01^{+0.34}_{-0.22}$	$0.46^{+0.24}_{-0.22}$	1.15	1.13	79.7
ABELL 0267 †	2.74	$6.70^{+0.56}_{-0.47}$	$8.88^{+1.68}_{-1.27}$	$1.33^{+0.27}_{-0.21}$	$0.32^{+0.11}_{-0.11}$	1.18	1.15	82.7

TABLE 4 — *Continued*

Cluster (1)	N_H 10^{20} cm^{-2} (2)	T_{77} keV (3)	T_{27} keV (4)	T_{HFR} (5)	Z_{77} $Z_\odot$ (6)	$\chi^2_{red,77}$ (7)	$\chi^2_{red,27}$ (8)	% Source (9)
ABELL 0370	3.37	$7.35^{+0.72}_{-0.84}$	$10.35^{+1.89}_{-2.27}$	$1.41^{+0.29}_{-0.35}$	$0.45^{+0.06}_{-0.23}$	1.08	1.04	39.2
ABELL 0383	4.07	$4.91^{+0.29}_{-0.27}$	$5.42^{+0.74}_{-0.59}$	$1.10^{+0.16}_{-0.13}$	$0.44^{+0.11}_{-0.11}$	0.97	0.90	64.2
ABELL 0399	$7.57^{+0.71}_{-0.71}$	$7.95^{+0.35}_{-0.31}$	$8.87^{+0.55}_{-0.50}$	$1.12^{+0.08}_{-0.08}$	$0.30^{+0.05}_{-0.05}$	1.12	0.99	82.2
ABELL 0520	$1.06^{+1.06}_{-1.05}$	$9.29^{+0.67}_{-0.60}$	$9.88^{+0.85}_{-0.73}$	$1.06^{+0.12}_{-0.10}$	$0.37^{+0.07}_{-0.07}$	1.11	1.04	87.6
ABELL 0521	6.17	$7.03^{+0.59}_{-0.53}$	$8.39^{+1.62}_{-1.22}$	$1.19^{+0.25}_{-0.20}$	$0.39^{+0.13}_{-0.12}$	1.10	1.15	49.5
ABELL 0586	4.71	$6.47^{+0.55}_{-0.47}$	$8.06^{+1.46}_{-1.11}$	$1.25^{+0.25}_{-0.19}$	$0.56^{+0.17}_{-0.16}$	0.91	0.81	82.0
ABELL 0611	4.99	$7.06^{+0.55}_{-0.48}$	$7.97^{+1.09}_{-0.91}$	$1.13^{+0.18}_{-0.15}$	$0.35^{+0.11}_{-0.10}$	0.97	0.98	54.2
ABELL 0665	4.24	$7.45^{+0.38}_{-0.34}$	$9.61^{+1.02}_{-0.85}$	$1.29^{+0.15}_{-0.13}$	$0.31^{+0.06}_{-0.07}$	1.02	0.93	87.7
ABELL 0697	3.34	$9.52^{+0.87}_{-0.76}$	$12.24^{+2.05}_{-1.63}$	$1.29^{+0.25}_{-0.20}$	$0.37^{+0.12}_{-0.11}$	1.08	1.02	89.4
ABELL 0773	1.46	$7.83^{+0.66}_{-0.57}$	$9.75^{+1.65}_{-1.27}$	$1.25^{+0.24}_{-0.19}$	$0.44^{+0.12}_{-0.12}$	1.06	1.09	84.0
ABELL 0781	1.90	$5.81^{+1.01}_{-0.79}$	$7.50^{+3.57}_{-1.81}$	$1.29^{+0.65}_{-0.36}$	$0.31^{+0.24}_{-0.20}$	1.38	1.61	74.1
ABELL 0907	5.69	$5.59^{+0.18}_{-0.18}$	$6.69^{+0.47}_{-0.42}$	$1.20^{+0.09}_{-0.08}$	$0.42^{+0.06}_{-0.05}$	1.13	0.99	88.0
ABELL 0963	1.39	$6.73^{+0.32}_{-0.30}$	$6.98^{+0.66}_{-0.57}$	$1.04^{+0.11}_{-0.10}$	$0.29^{+0.07}_{-0.08}$	1.06	1.02	64.9
ABELL 1063S	1.77	$11.96^{+0.88}_{-0.79}$	$13.70^{+1.68}_{-1.38}$	$1.15^{+0.16}_{-0.14}$	$0.38^{+0.09}_{-0.09}$	1.02	0.98	90.6
ABELL 1068	0.71	$4.62^{+0.18}_{-0.18}$	$5.17^{+0.51}_{-0.43}$	$1.12^{+0.12}_{-0.10}$	$0.34^{+0.06}_{-0.07}$	1.00	1.01	68.4
ABELL 1204	1.44	$3.63^{+0.16}_{-0.16}$	$4.58^{+0.57}_{-0.45}$	$1.26^{+0.17}_{-0.14}$	$0.31^{+0.09}_{-0.09}$	1.06	0.90	88.3
ABELL 1423	1.60	$6.01^{+0.75}_{-0.64}$	$7.53^{+2.35}_{-1.55}$	$1.25^{+0.42}_{-0.29}$	$0.30^{+0.18}_{-0.17}$	0.87	0.65	78.3
ABELL 1651	2.02	$6.26^{+0.30}_{-0.27}$	$7.78^{+0.90}_{-0.76}$	$1.24^{+0.16}_{-0.13}$	$0.42^{+0.09}_{-0.09}$	1.19	1.20	86.6
ABELL 1664	8.47	$4.39^{+0.30}_{-0.28}$	$5.20^{+0.92}_{-0.71}$	$1.18^{+0.22}_{-0.18}$	$0.26^{+0.11}_{-0.10}$	0.98	0.99	61.3
ABELL 1682	1.10	$7.06^{+1.76}_{-1.26}$	$10.30^{+8.85}_{-3.42}$	$1.46^{+1.31}_{-0.55}$	$0.60^{+0.40}_{-0.33}$	1.19	1.33	64.0
ABELL 1689	1.87	$9.46^{+0.54}_{-0.48}$	$13.23^{+1.87}_{-1.47}$	$1.40^{+0.21}_{-0.17}$	$0.38^{+0.07}_{-0.08}$	1.31	1.16	91.1
ABELL 1758	1.09	$12.14^{+1.15}_{-0.92}$	$11.16^{+3.08}_{-2.14}$	$0.92^{+0.27}_{-0.19}$	$0.56^{+0.13}_{-0.13}$	1.21	1.09	58.3
ABELL 1763	0.82	$7.78^{+0.67}_{-0.60}$	$11.49^{+2.89}_{-1.84}$	$1.48^{+0.39}_{-0.26}$	$0.25^{+0.10}_{-0.10}$	1.12	0.92	84.7
ABELL 1835	2.36	$9.77^{+0.57}_{-0.52}$	$11.00^{+1.23}_{-1.03}$	$1.13^{+0.14}_{-0.12}$	$0.31^{+0.08}_{-0.07}$	0.98	1.02	86.5
ABELL 1914	0.97	$9.62^{+0.55}_{-0.49}$	$11.42^{+1.26}_{-1.06}$	$1.19^{+0.15}_{-0.13}$	$0.30^{+0.08}_{-0.07}$	1.07	1.03	92.0
ABELL 1942	2.75	$4.77^{+0.38}_{-0.35}$	$5.49^{+0.98}_{-0.74}$	$1.15^{+0.22}_{-0.18}$	$0.33^{+0.12}_{-0.14}$	1.06	1.04	70.1
ABELL 2034	1.58	$7.15^{+0.23}_{-0.22}$	$10.02^{+0.92}_{-0.75}$	$1.40^{+0.14}_{-0.11}$	$0.32^{+0.05}_{-0.05}$	1.22	1.00	84.6
ABELL 2069	1.97	$6.50^{+0.33}_{-0.29}$	$8.61^{+1.02}_{-0.84}$	$1.32^{+0.17}_{-0.14}$	$0.26^{+0.08}_{-0.07}$	1.04	0.96	71.4
ABELL 2111	2.20	$7.13^{+1.29}_{-0.95}$	$11.10^{+4.67}_{-3.05}$	$1.56^{+0.71}_{-0.48}$	$0.13^{+0.19}_{-0.13}$	1.06	0.88	76.3
ABELL 2125	2.75	$2.88^{+0.30}_{-0.27}$	$3.76^{+0.98}_{-0.65}$	$1.31^{+0.37}_{-0.26}$	$0.31^{+0.18}_{-0.16}$	1.26	1.30	61.8
ABELL 2163	12.04	$19.20^{+0.87}_{-0.80}$	$21.30^{+1.77}_{-1.47}$	$1.11^{+0.11}_{-0.09}$	$0.10^{+0.06}_{-0.06}$	1.37	1.26	90.0
ABELL 2218	3.12	$7.35^{+0.39}_{-0.35}$	$10.03^{+1.26}_{-0.98}$	$1.36^{+0.19}_{-0.15}$	$0.22^{+0.07}_{-0.06}$	1.01	0.90	87.6
ABELL 2219	1.76	$12.75^{+0.64}_{-0.59}$	$12.39^{+1.09}_{-0.93}$	$0.97^{+0.10}_{-0.09}$	$0.28^{+0.07}_{-0.07}$	1.01	1.00	75.3
ABELL 2255	2.53	$6.12^{+0.20}_{-0.19}$	$8.10^{+0.66}_{-0.58}$	$1.32^{+0.12}_{-0.10}$	$0.30^{+0.06}_{-0.06}$	1.13	0.95	76.8
ABELL 2259	3.70	$5.18^{+0.46}_{-0.39}$	$6.40^{+1.33}_{-0.95}$	$1.24^{+0.28}_{-0.21}$	$0.41^{+0.14}_{-0.14}$	1.05	1.01	85.6
ABELL 2261	3.31	$7.63^{+0.47}_{-0.43}$	$9.30^{+1.21}_{-0.91}$	$1.22^{+0.18}_{-0.14}$	$0.36^{+0.08}_{-0.08}$	0.99	0.95	90.1
ABELL 2294	6.10	$9.98^{+1.43}_{-1.12}$	$11.07^{+3.19}_{-2.11}$	$1.11^{+0.36}_{-0.25}$	$0.53^{+0.21}_{-0.21}$	1.07	0.95	82.8
ABELL 2384	2.99	$4.75^{+0.23}_{-0.20}$	$6.22^{+0.72}_{-0.60}$	$1.31^{+0.16}_{-0.14}$	$0.23^{+0.07}_{-0.07}$	1.06	0.92	81.6
ABELL 2390	6.71	$11.15^{+0.34}_{-0.32}$	$11.17^{+0.58}_{-0.51}$	$1.00^{+0.06}_{-0.05}$	$0.36^{+0.04}_{-0.04}$	1.20	1.08	74.3
ABELL 2409	6.72	$5.94^{+0.43}_{-0.38}$	$6.77^{+0.99}_{-0.82}$	$1.14^{+0.19}_{-0.16}$	$0.37^{+0.13}_{-0.11}$	1.13	0.96	88.3
ABELL 2537	4.26	$8.40^{+0.76}_{-0.68}$	$7.81^{+1.15}_{-0.93}$	$0.93^{+0.16}_{-0.13}$	$0.40^{+0.13}_{-0.13}$	0.91	0.84	46.5
ABELL 2550	2.03	$2.06^{+0.12}_{-0.11}$	$2.17^{+0.46}_{-0.33}$	$1.05^{+0.23}_{-0.17}$	$0.33^{+0.09}_{-0.08}$	1.26	1.11	34.3
ABELL 2667	1.64	$6.75^{+0.48}_{-0.43}$	$7.45^{+1.06}_{-0.88}$	$1.10^{+0.18}_{-0.15}$	$0.36^{+0.11}_{-0.11}$	1.17	1.08	76.4
ABELL 2670	2.88	$3.95^{+0.14}_{-0.12}$	$4.65^{+0.42}_{-0.36}$	$1.18^{+0.11}_{-0.19}$	$0.42^{+0.08}_{-0.06}$	1.13	1.07	70.8
ABELL 2744	1.82	$9.18^{+0.68}_{-0.60}$	$10.20^{+1.38}_{-1.10}$	$1.11^{+0.17}_{-0.14}$	$0.24^{+0.10}_{-0.09}$	0.99	0.90	67.5
AC 114	1.44	$7.53^{+0.49}_{-0.44}$	$8.30^{+1.03}_{-0.85}$	$1.10^{+0.15}_{-0.13}$	$0.26^{+0.08}_{-0.09}$	1.07	1.06	55.7
CL 0024+17	4.36	$6.03^{+1.66}_{-1.10}$	$7.18^{+7.91}_{-3.16}$	$1.19^{+1.35}_{-0.57}$	$0.60^{+0.37}_{-0.33}$	1.00	1.44	37.1
CL 1221+4918	1.44	$6.62^{+1.24}_{-0.99}$	$7.11^{+1.73}_{-1.31}$	$1.07^{+0.33}_{-0.25}$	$0.34^{+0.20}_{-0.18}$	0.94	0.93	62.2
CL J0030+2618	4.10	$4.63^{+2.72}_{-1.32}$	$5.18^{+8.29}_{-1.96}$	$1.12^{+1.91}_{-0.53}$	$0.26^{+0.75}_{-0.26}$	1.00	1.23	37.7
CL J0152-1357	1.45	$7.33^{+2.78}_{-1.77}$	$7.31^{+3.43}_{-2.02}$	$1.00^{+0.60}_{-0.37}$	$0.00^{+0.24}_{-0.00}$	0.89	1.00	36.2
CL J0542.8-4100	3.59	$6.07^{+1.47}_{-1.05}$	$6.29^{+2.14}_{-1.41}$	$1.04^{+0.43}_{-0.29}$	$0.16^{+0.23}_{-0.16}$	1.04	0.91	66.4
CL J0848+4456 †	2.53	$4.53^{+1.57}_{-1.13}$	$5.52^{+3.28}_{-1.74}$	$1.22^{+0.84}_{-0.49}$	$0.00^{+0.45}_{-0.00}$	0.92	0.93	58.3
CL J1113.1-2615	5.51	$4.19^{+1.61}_{-1.02}$	$4.10^{+2.47}_{-1.44}$	$0.98^{+0.70}_{-0.42}$	$0.46^{+0.63}_{-0.44}$	1.01	1.08	23.7
CL J1213+0253	$0.02^{+23.12}_{-0.02}$	$4.62^{+2.78}_{-2.29}$	$4.10^{+3.54}_{-1.83}$	$0.89^{+0.93}_{-0.59}$	$0.00^{+1.15}_{-0.00}$	0.50	0.64	51.9
CL J1226.9+3332 †	1.37	$11.81^{+2.25}_{-1.70}$	$11.29^{+2.45}_{-1.77}$	$0.96^{+0.28}_{-0.20}$	$0.21^{+0.21}_{-0.21}$	0.81	0.86	86.7
CL J1641+4001	1.09	$3.29^{+0.93}_{-0.54}$	$5.75^{+3.80}_{-2.01}$	$1.75^{+1.26}_{-0.67}$	$0.77^{+0.92}_{-0.59}$	1.63	1.77	74.8
CL J2302.8+0844	5.05	$4.25^{+1.17}_{-1.32}$	$4.67^{+2.00}_{-1.80}$	$1.10^{+0.56}_{-0.54}$	$0.13^{+0.33}_{-0.13}$	0.89	0.97	50.7
IRAS 09104+4109	1.36	$8.06^{+3.25}_{-2.02}$	$6.31^{+4.36}_{-3.22}$	$0.78^{+0.63}_{-0.45}$	$1.03^{+0.73}_{-0.56}$	0.85	0.89	82.8
LYNX E †	2.53	$7.63^{+8.61}_{-3.18}$	$8.86^{+\infty}_{-4.40}$	$1.16^{+3.33}_{-0.75}$	$0.00^{+0.64}_{-0.00}$	0.81	1.02	61.2
MACS J0011.7-1523	2.08	$6.64^{+0.62}_{-0.53}$	$6.90^{+1.05}_{-0.82}$	$1.04^{+0.19}_{-0.15}$	$0.32^{+0.12}_{-0.12}$	0.90	0.87	81.7
MACS J0025.4-1222 †	2.72	$6.33^{+0.85}_{-0.70}$	$6.01^{+1.05}_{-0.85}$	$0.95^{+0.21}_{-0.17}$	$0.37^{+0.16}_{-0.15}$	0.90	0.92	80.4
MACS J0159.8-0849 †	2.01	$9.16^{+0.71}_{-0.63}$	$9.83^{+1.13}_{-0.96}$	$1.07^{+0.15}_{-0.13}$	$0.30^{+0.09}_{-0.09}$	1.08	1.09	90.6
MACS J0242.5-2132	2.71	$5.58^{+0.63}_{-0.52}$	$6.26^{+1.38}_{-0.99}$	$1.12^{+0.21}_{-0.16}$	$0.34^{+0.16}_{-0.15}$	1.03	0.83	87.2
MACS J0257.1-2325 †	2.09	$9.25^{+1.28}_{-1.01}$	$10.16^{+1.95}_{-1.54}$	$1.10^{+0.26}_{-0.21}$	$0.14^{+0.12}_{-0.12}$	0.99	1.08	84.7

TABLE 4 — *Continued*

Cluster	N_H 10^{20} cm^{-2}	T_{77} keV	T_{27} keV	T_{HFR}	Z_{77} $Z_\odot$	$\chi^2_{red,77}$	$\chi^2_{red,27}$	% Source
(1)	(2)	(3)	(4)	(5)	(6)	(7)	(8)	(9)
MACS J0257.6-2209	2.02	$8.02^{+1.12}_{-0.88}$	$8.17^{+1.92}_{-1.30}$	$1.02^{+0.28}_{-0.20}$	$0.30^{+0.16}_{-0.17}$	1.12	1.26	84.5
MACS J0329.6-0211 †	6.21	$6.30^{+0.47}_{-0.41}$	$7.50^{+0.83}_{-0.69}$	$1.19^{+0.16}_{-0.13}$	$0.41^{+0.10}_{-0.09}$	1.10	1.17	86.4
MACS J0404.6+1109	14.96	$5.77^{+1.14}_{-0.88}$	$6.15^{+2.00}_{-1.30}$	$1.07^{+0.41}_{-0.28}$	$0.24^{+0.22}_{-0.20}$	0.85	0.78	73.7
MACS J0417.5-1154	4.00	$11.07^{+1.98}_{-1.49}$	$14.90^{+5.03}_{-3.24}$	$1.35^{+0.51}_{-0.34}$	$0.33^{+0.19}_{-0.19}$	1.07	0.97	94.8
MACS J0429.6-0253	5.70	$5.66^{+0.64}_{-0.54}$	$6.71^{+1.26}_{-0.98}$	$1.19^{+0.26}_{-0.21}$	$0.35^{+0.14}_{-0.13}$	1.21	1.12	82.7
MACS J0451.9+0006	7.65	$5.80^{+1.46}_{-1.03}$	$7.02^{+3.29}_{-1.80}$	$1.21^{+0.64}_{-0.38}$	$0.51^{+0.33}_{-0.29}$	1.25	1.35	83.8
MACS J0547.0-3904	4.08	$3.58^{+0.44}_{-0.37}$	$5.41^{+1.67}_{-1.18}$	$1.51^{+0.50}_{-0.36}$	$0.09^{+0.15}_{-0.09}$	1.16	1.42	75.5
MACS J0717.5+3745 †	6.75	$12.77^{+1.16}_{-1.00}$	$13.21^{+1.58}_{-1.29}$	$1.03^{+0.16}_{-0.13}$	$0.30^{+0.10}_{-0.10}$	0.93	0.90	88.1
MACS J0744.8+3927 †	4.66	$8.09^{+0.77}_{-0.66}$	$8.77^{+1.04}_{-0.87}$	$1.08^{+0.16}_{-0.14}$	$0.32^{+0.10}_{-0.10}$	1.14	1.18	82.9
MACS J0911.2+1746	3.55	$8.30^{+2.64}_{-1.67}$	$8.66^{+4.42}_{-2.26}$	$1.04^{+0.63}_{-0.34}$	$0.21^{+0.28}_{-0.21}$	0.69	0.76	78.3
MACS J0949+1708	3.17	$9.16^{+1.53}_{-1.18}$	$9.11^{+2.27}_{-1.55}$	$0.99^{+0.30}_{-0.21}$	$0.37^{+0.20}_{-0.20}$	0.89	0.84	89.1
MACS J1115.8+0129	4.36	$6.78^{+1.17}_{-0.91}$	$8.27^{+3.27}_{-2.16}$	$1.22^{+0.53}_{-0.36}$	$0.07^{+0.21}_{-0.07}$	1.00	0.97	65.9
MACS J1131.8-1955	4.49	$8.64^{+1.23}_{-0.97}$	$11.01^{+3.61}_{-2.10}$	$1.27^{+0.46}_{-0.28}$	$0.42^{+0.17}_{-0.17}$	1.00	1.00	87.4
MACS J1149.5+2223 †	2.32	$6.20^{+0.71}_{-0.57}$	$11.88^{+4.64}_{-2.71}$	$1.92^{+0.78}_{-0.47}$	$0.21^{+0.14}_{-0.14}$	1.05	1.04	71.6
MACS J1206.2-0847	4.15	$10.21^{+1.19}_{-0.97}$	$12.51^{+2.44}_{-1.87}$	$1.23^{+0.28}_{-0.22}$	$0.33^{+0.13}_{-0.13}$	0.96	1.05	93.1
MACS J1226.8+2153	1.82	$4.21^{+1.07}_{-0.80}$	$5.02^{+3.29}_{-1.52}$	$1.19^{+0.84}_{-0.43}$	$0.23^{+0.38}_{-0.23}$	1.02	0.81	67.9
MACS J1311.0-0310 †	2.18	$5.76^{+0.48}_{-0.42}$	$5.91^{+0.73}_{-0.62}$	$1.03^{+0.15}_{-0.13}$	$0.39^{+0.13}_{-0.11}$	0.96	0.98	72.0
MACS J1319+7003	1.53	$7.99^{+2.08}_{-1.43}$	$10.62^{+7.35}_{-3.22}$	$1.33^{+0.98}_{-0.47}$	$0.30^{+0.29}_{-0.28}$	1.25	1.24	74.4
MACS J1427.6-2521	6.11	$4.66^{+0.95}_{-0.72}$	$8.37^{+5.00}_{-2.96}$	$1.80^{+1.13}_{-0.69}$	$0.18^{+0.27}_{-0.18}$	1.19	1.39	68.9
MACS J1621.3+3810 †	1.07	$7.12^{+0.66}_{-0.55}$	$7.09^{+0.92}_{-0.75}$	$1.00^{+0.16}_{-0.13}$	$0.34^{+0.11}_{-0.11}$	0.93	0.86	73.4
MACS J1824.3+4309	4.52	$5.53^{+4.46}_{-1.87}$	$12.32^{+\infty}_{-6.86}$	$2.23^{+10.17}_{-1.45}$	$0.47^{+1.06}_{-0.47}$	1.48	0.95	71.9
MACS J1931.8-2634	9.13	$6.97^{+0.72}_{-0.61}$	$7.72^{+1.31}_{-0.99}$	$1.11^{+0.22}_{-0.17}$	$0.27^{+0.11}_{-0.12}$	0.95	0.86	90.4
MACS J2211.7-0349	5.86	$11.30^{+1.46}_{-1.17}$	$13.82^{+3.54}_{-2.41}$	$1.22^{+0.35}_{-0.25}$	$0.15^{+0.13}_{-0.14}$	1.24	1.26	88.4
MACS J2214.9-1359 †	3.32	$9.78^{+1.38}_{-1.09}$	$10.45^{+2.19}_{-1.56}$	$1.07^{+0.27}_{-0.20}$	$0.23^{+0.14}_{-0.14}$	0.99	1.06	87.8
MACS J2228+2036	4.52	$7.86^{+1.08}_{-0.85}$	$9.17^{+2.05}_{-1.46}$	$1.17^{+0.31}_{-0.22}$	$0.39^{+0.16}_{-0.15}$	0.99	1.00	88.2
MACS J2229.7-2755	1.34	$5.01^{+0.50}_{-0.43}$	$5.79^{+1.11}_{-0.86}$	$1.16^{+0.25}_{-0.20}$	$0.55^{+0.19}_{-0.18}$	1.05	1.08	85.4
MACS J2245.0+2637	5.50	$6.06^{+0.63}_{-0.54}$	$6.76^{+1.24}_{-0.93}$	$1.12^{+0.24}_{-0.18}$	$0.60^{+0.20}_{-0.18}$	0.94	1.09	88.1
MACS J2311+0338	5.23	$8.14^{+1.45}_{-1.16}$	$12.53^{+5.10}_{-2.93}$	$1.54^{+0.68}_{-0.42}$	$0.46^{+0.22}_{-0.20}$	1.07	1.15	88.7
MS 0016.9+1609	4.06	$8.94^{+0.71}_{-0.62}$	$9.78^{+1.09}_{-0.90}$	$1.09^{+0.15}_{-0.13}$	$0.29^{+0.09}_{-0.08}$	0.91	0.88	83.5
MS 0302.7+1658	10.95	$3.27^{+1.05}_{-0.64}$	$2.60^{+1.23}_{-0.55}$	$0.80^{+0.45}_{-0.23}$	$0.81^{+1.56}_{-0.73}$	1.14	1.12	70.9
MS 0451.6-0305	5.68	$8.90^{+0.85}_{-0.72}$	$10.43^{+1.59}_{-1.26}$	$1.17^{+0.21}_{-0.17}$	$0.37^{+0.11}_{-0.11}$	1.00	0.93	60.8
MS 0735.6+7421	3.40	$5.55^{+0.24}_{-0.22}$	$6.34^{+0.57}_{-0.50}$	$1.14^{+0.11}_{-0.10}$	$0.35^{+0.07}_{-0.06}$	1.05	1.05	62.9
MS 0839.8+2938	3.92	$4.68^{+0.32}_{-0.29}$	$5.05^{+0.82}_{-0.65}$	$1.08^{+0.19}_{-0.15}$	$0.46^{+0.13}_{-0.12}$	0.90	0.87	60.8
MS 0906.5+1110	3.60	$5.38^{+0.33}_{-0.29}$	$6.76^{+0.92}_{-0.77}$	$1.26^{+0.19}_{-0.16}$	$0.27^{+0.09}_{-0.09}$	1.21	1.08	75.5
MS 1006.0+1202	3.63	$5.61^{+0.51}_{-0.43}$	$7.48^{+1.66}_{-1.22}$	$1.33^{+0.32}_{-0.24}$	$0.24^{+0.11}_{-0.12}$	1.30	1.34	75.5
MS 1008.1-1224	$0.00^{+1.29}_{-0.00}$	$7.45^{+0.80}_{-0.71}$	$9.22^{+2.05}_{-1.43}$	$1.24^{+0.31}_{-0.23}$	$0.29^{+0.13}_{-0.13}$	1.10	0.98	78.9
MS 1054.5-0321	3.69	$9.38^{+1.72}_{-1.34}$	$9.91^{+2.66}_{-1.77}$	$1.06^{+0.34}_{-0.24}$	$0.13^{+0.17}_{-0.13}$	1.02	1.03	41.6
MS 1455.0+2232	3.35	$4.77^{+0.13}_{-0.13}$	$5.37^{+0.36}_{-0.22}$	$1.13^{+0.08}_{-0.06}$	$0.44^{+0.06}_{-0.05}$	1.29	1.10	90.5
MS 1621.5+2640	3.59	$6.11^{+0.95}_{-0.76}$	$6.22^{+1.56}_{-1.10}$	$1.02^{+0.30}_{-0.22}$	$0.40^{+0.23}_{-0.21}$	1.02	1.21	68.0
MS 2053.7-0449 †	5.16	$3.66^{+0.81}_{-0.60}$	$4.07^{+1.23}_{-0.83}$	$1.11^{+0.42}_{-0.29}$	$0.39^{+0.38}_{-0.35}$	0.97	1.07	58.9
MS 2137.3-2353	3.40	$6.01^{+0.52}_{-0.46}$	$7.48^{+1.68}_{-1.09}$	$1.24^{+0.30}_{-0.20}$	$0.45^{+0.13}_{-0.13}$	1.12	1.25	55.6
RBS 0797	2.22	$7.68^{+0.92}_{-0.77}$	$9.05^{+1.80}_{-1.33}$	$1.18^{+0.27}_{-0.21}$	$0.32^{+0.14}_{-0.13}$	1.07	1.06	89.0
RDCS 1252-29	6.06	$4.25^{+1.82}_{-1.14}$	$4.47^{+2.16}_{-1.29}$	$1.05^{+0.68}_{-0.41}$	$0.79^{+1.01}_{-0.62}$	1.07	1.17	50.7
RX J0439+0520	10.02	$4.60^{+0.64}_{-0.59}$	$4.95^{+1.28}_{-0.88}$	$1.08^{+0.32}_{-0.24}$	$0.44^{+0.29}_{-0.24}$	1.03	1.14	77.8
RX J0439.0+0715 †	11.16	$5.63^{+0.36}_{-0.32}$	$8.02^{+1.25}_{-0.93}$	$1.42^{+0.24}_{-0.18}$	$0.32^{+0.10}_{-0.08}$	1.28	1.16	82.8
RX J0647.7+7015 †	5.18	$11.28^{+1.85}_{-1.45}$	$11.01^{+2.17}_{-1.63}$	$0.98^{+0.25}_{-0.19}$	$0.20^{+0.11}_{-0.17}$	1.02	1.00	80.7
RX J0910+5422 †	2.07	$4.53^{+3.02}_{-1.70}$	$5.98^{+5.30}_{-2.49}$	$1.32^{+1.46}_{-0.74}$	$0.00^{+0.73}_{-0.00}$	0.90	0.71	31.4
RX J1053+5735	0.59	$7.03^{+17.25}_{-3.46}$	$5.06^{+12.74}_{-2.48}$	$0.72^{+2.53}_{-0.50}$	$0.55^{+2.26}_{-0.55}$	1.48	1.27	16.8
RX J1347.5-1145 †	4.89	$14.62^{+0.97}_{-0.79}$	$16.62^{+1.54}_{-1.24}$	$1.14^{+0.13}_{-0.10}$	$0.32^{+0.08}_{-0.07}$	1.12	1.12	93.1
RX J1350+6007	1.77	$4.48^{+2.32}_{-1.49}$	$5.31^{+3.02}_{-2.07}$	$1.19^{+0.91}_{-0.61}$	$0.13^{+1.23}_{-0.13}$	0.82	0.72	57.6
RX J1423.8+2404 †	2.65	$6.64^{+0.38}_{-0.34}$	$7.01^{+0.59}_{-0.51}$	$1.06^{+0.11}_{-0.09}$	$0.37^{+0.07}_{-0.07}$	1.02	0.98	86.0
RX J1504.1-0248	6.27	$8.00^{+0.27}_{-0.24}$	$8.92^{+0.59}_{-0.46}$	$1.11^{+0.08}_{-0.07}$	$0.40^{+0.05}_{-0.05}$	1.29	1.25	91.9
RX J1525+0958	2.96	$3.67^{+0.60}_{-0.44}$	$6.70^{+2.72}_{-1.57}$	$1.83^{+0.80}_{-0.48}$	$0.68^{+0.36}_{-0.29}$	1.27	0.93	78.1
RX J1532.9+3021 †	2.21	$6.03^{+0.42}_{-0.38}$	$6.95^{+0.88}_{-0.72}$	$1.15^{+0.14}_{-0.14}$	$0.42^{+0.11}_{-0.10}$	0.94	1.05	73.8
RX J1716.9+6708	3.71	$5.71^{+1.47}_{-1.06}$	$5.77^{+1.88}_{-1.28}$	$1.01^{+0.42}_{-0.29}$	$0.68^{+0.42}_{-0.35}$	0.79	0.74	55.3
RX J1720.1+2638	4.02	$6.37^{+0.28}_{-0.26}$	$7.78^{+0.69}_{-0.61}$	$1.22^{+0.12}_{-0.11}$	$0.35^{+0.07}_{-0.07}$	1.10	1.02	90.7
RX J1720.2+3536 †	3.35	$7.21^{+0.53}_{-0.46}$	$6.97^{+0.76}_{-0.59}$	$0.97^{+0.13}_{-0.10}$	$0.41^{+0.10}_{-0.10}$	1.12	1.09	85.5
RX J2129.6+0005	4.30	$5.91^{+0.54}_{-0.47}$	$7.02^{+1.30}_{-0.99}$	$1.19^{+0.25}_{-0.19}$	$0.45^{+0.15}_{-0.15}$	1.21	1.07	80.9
V 1121.0+2327	1.30	$3.60^{+0.62}_{-0.46}$	$4.08^{+1.09}_{-0.80}$	$1.13^{+0.36}_{-0.27}$	$0.36^{+0.29}_{-0.24}$	1.21	1.19	66.3
ZWCL 1215	1.76	$6.62^{+0.39}_{-0.36}$	$8.67^{+1.29}_{-1.06}$	$1.31^{+0.21}_{-0.18}$	$0.29^{+0.09}_{-0.09}$	1.17	1.04	88.4
ZWCL 1358+6245	1.94	$10.66^{+1.48}_{-1.13}$	$10.19^{+4.83}_{-2.24}$	$0.96^{+0.47}_{-0.23}$	$0.47^{+0.19}_{-0.19}$	1.08	1.04	55.5
ZWCL 1953	3.10	$7.37^{+1.00}_{-0.78}$	$10.44^{+3.25}_{-2.20}$	$1.42^{+0.48}_{-0.33}$	$0.19^{+0.13}_{-0.13}$	0.84	0.78	74.1
ZWCL 3146	2.70	$7.48^{+0.32}_{-0.30}$	$8.61^{+0.66}_{-0.58}$	$1.15^{+0.10}_{-0.09}$	$0.31^{+0.05}_{-0.06}$	1.03	0.98	86.2
ZWCL 5247	1.70	$5.06^{+0.85}_{-0.64}$	$5.91^{+2.09}_{-1.30}$	$1.17^{+0.46}_{-0.30}$	$0.22^{+0.21}_{-0.19}$	0.83	0.72	74.2

TABLE 4 — *Continued*

Cluster	N_H	T_{77}	T_{27}	T_{HFR}		Z_{77}	$\chi^2_{red,77}$	$\chi^2_{red,27}$	% Source
	10^{20} cm^{-2}	keV	keV			$Z_\odot$			
(1)	(2)	(3)	(4)	(5)		(6)	(7)	(8)	(9)
ZWCL 7160	3.10	$4.53^{+0.40}_{-0.35}$	$5.16^{+1.01}_{-0.77}$	$1.14^{+0.24}_{-0.19}$		$0.40^{+0.15}_{-0.14}$	0.94	0.92	80.7
ZWICKY 2701	0.83	$5.21^{+0.34}_{-0.30}$	$5.68^{+0.85}_{-0.66}$	$1.09^{+0.18}_{-0.14}$		$0.43^{+0.13}_{-0.11}$	0.89	0.94	57.8
ZwCL 1332.8+5043	1.10	$3.62^{+3.46}_{-1.20}$	$3.84^{+5.93}_{-1.48}$	$1.06^{+1.93}_{-0.54}$		$0.76^{+12.45}_{-0.76}$	0.24	0.29	48.4

NOTE. — Note: '77' refers to 0.7-7.0 keV band, '27' refers to 2.0$_{rest}$-7.0 keV band. (1) Cluster name, (2) absorbing, Galactic neutral hydrogen column density, (3,4) best-fit MeKaL temperatures, (5) best-fit 77 MeKaL abundance, (6) T_{HFR}, (7,8) reduced χ^2 statistics, (9) percent of emission attributable to source. † indicates cluster with multiple independent, simultaneously fit spectra.